Deliverable Report D1.44

PI-based assessment of most promising concepts combined with advanced control

Agreement n.:	308974
Duration	November 2012 – October 2017
Co-ordinator:	DTU Wind

The research leading to these results has received funding from the European Community's Seventh Framework Programme FP7-ENERGY-2012-1-2STAGE under grant agreement No. 308974 (INNWIND.EU)

Document information

Document Name:	D1.44 PI-based assessment of most promising concepts combined with advanced control
Document Number:	Deliverable D 1.44
Author:	Anand Natarajan, Athanasios Barlas, Davide Conti (DTU) Avishek Kumar, Oscar Hughes Salas (DNV GL) Vasilis Riziotis (NTUA), Dimitris Manolas (NTUA) Stoyan Kanev (ECN)
Document Type	Report
Dissemination level	PU
Review:	Takis Chaviaropoulos
Date:	Aug 30, 2017
WP:	1
Task:	4
Approval:	Approved by WP Leader

Table of Contents

1.0 Overview of Chosen Concepts for Evaluation (DTU) 5
2.0 Evaluation of 10 MW Floating Horizontal Axis Wind Turbine with advanced control (NTUA) 6
3.0 Evaluation of 10 MW 2 Bladed Semi Floater with Optimized Blades (DTU) 15
3.1 Design loads and sensors 15
3.2 Power Curve 16
3.3 Ultimate limit state 17
3.4 Fatigue limit state 22
3.5 Discussion 27
4.0 Evaluation of 20 MW on Jacket with Flap control (GL-GH, now DNV GL (UK)) 28
4.1 Modelling of the 20 MW Reference Turbine with Flaps 29
4.1.1 Simulation and Analysis Tools 29
4.1.2 Reference 20 MW 30
4.2 Results 35
4.3 Conclusions 40
5.0 Evaluation of 20 MW LIR Wind Turbine with advanced control (NTUA) 41
6.0 Evaluation of 20 MW Wind Turbine with Extreme Turbulence control (ECN) 49
5.1 Extreme turbulence control 50
5.1.1 Turbulence estimation 51
5.1.2 Extreme turbulence detection 52
5.1.3 Threshold optimization 53
5.2 Results 55
5.2.1 Test case INNWIND.EU 10MW reference turbine 55
5.2.2 Test case INNWIND.EU 20MW reference turbine 61
5.3 Discussion 66

7.0 Quantification of LCOE Reduction of Innovations at 10 MW and 20 MW Scale with Advanced Control (ALL) 67
8.0 Conclusions 68
Bibliography 69
Appendix A Load case definition for 20 MW Reference Turbine (GL-GH, now DNV GL (UK)) 71
General Comments 71
Fatigue Load Cases 71
Extreme Load Cases 76

1.0 Overview of Chosen Concepts for Evaluation (DTU)

This report provides a simulation based assessment of controller designs for innovative wind turbine concepts to ascertain the suitability of the controls in lowering the Levelized Cost of Energy (LCOE) under different operating conditions.

The chosen set of innovations includes:

1. 10 MW Floating wind turbine on a triple semi-submersible
2. The 20 MW reference wind turbine on a jacket
3. The 20 MW Low induction rotor turbine on a jacket
4. 2 Bladed 10 MW wind turbine on a Semi-Floater

The above innovative configurations were chosen in conjunction with deliverables D1.24 and D1.25 as some of the most effective systems for reducing LCOE. There are also 3 types of support structures that are investigated, 2 types of rotors (low induction and high performance) and 2-bladed versus 3-bladed rotors. So it is envisaged that the above 4 innovations encompass a significant part of the innovations developed within the INNWIND.EU project.

2.0 Evaluation of 10 MW Floating Horizontal Axis Wind Turbine with advanced control (NTUA)

In the present section, assessment of load reduction capabilities of an advanced control strategy applied to the floating DTU 10MW RWT mounted on the semi-submersible floater designed and developed under WP4 [**1**], is performed.

The block diagram of the controller is illustrated in Figure 1. Combined Individual trailing edge (TE) flap control (IFC) and individual pitch control (IPC) have been superimposed on the standard power speed controller of the INNWIND.EU 10MW RWT with the aim to alleviate blade loads. A standard individual flap/pitch control strategy has been employed as described in [**2**] [**3**]. As shown in Figure 1, the blade root out-of-plane bending moment signals are transformed into yaw and tilt moments Myaw and Mtilt by applying the Coleman transformation. 3p and 6p band-stop filters are applied to Myaw and Mtilt. The filtered moments are then passed through integral control elements (I) and cyclic flap/pitch angles are obtained. These angles are then back transformed into flap angles β_f and pitch angles β_p of the individual blades via an inverse Coleman transformation. In the IFC&IPC controller, flap control is supported by simultaneous individual control of the pitch angle of the three blades. Additional control logic with the aim to mitigate tower loads is added. Generator torque control and collective flap control is added based on the low pass filtered (0.3 Hz low pass frequency) tower top acceleration (with respect to tower bottom acceleration). Gains of the various integral control elements are provided in Table 1.

Trailing edge (TE) flap control is performed on the outer part of the blade of the DTU 10MW RWT. The blade of the reference turbine comprises FFA series airfoils. The relative thickness of the outer 35% of the blade is constant and equal to t/c=0.24. The camber line morphing shape presented in [**4**] is used. The flap extends to 30% of the section chord length. The spanwise extent of the flap is 34% of the blade radius. The basic characteristics of the flap are detailed in Table 2. Flap motion is bounded in the range $[-10^0, +10^0]$. In addition, saturation limits have been imposed on the velocity of the flap motion to 200/s. In all configurations a delay of 0.1 s has been imposed on the flap motion in order to account for the dynamics of the flap actuator (through a first order filter in flap response).

Both fatigue and ultimate loads are considered in the analyses. Fatigue loads are assessed on the basis of IEC DLC 1.2 (normal operation with normal turbulence conditions NTM and normal sea state NSS) while ultimate loads are estimated through DLC 1.3 (normal operation with extreme turbulence conditions ETM and NSS) and DLC 1.6 (NTM combined with severe sea state SSS). Simulated conditions and wind speeds are summarized in Table 3. It is noted that for all wind speeds 1 h simulations have been performed. In Table 4, wave characteristics (in terms of significant wave height Hs and peak spectral period Tp) used in the simulations are provided for the different sea conditions and wind speeds.

For the IA 10MW RWT mounted on the floating base, simulations are performed (a) for the baseline turbine with the standard power speed controller (thereafter called "default"), (b) for the turbine with advanced aeroelastic control (thereafter called "ipc_ifc_gen_flap"). The aim of the analysis is to assess load reduction capabilities of the advanced aeroelastic control strategy on floating turbines. Lifetime fatigue loads are calculated assuming the following Weibull parameters: C=11 m/s and k=2.

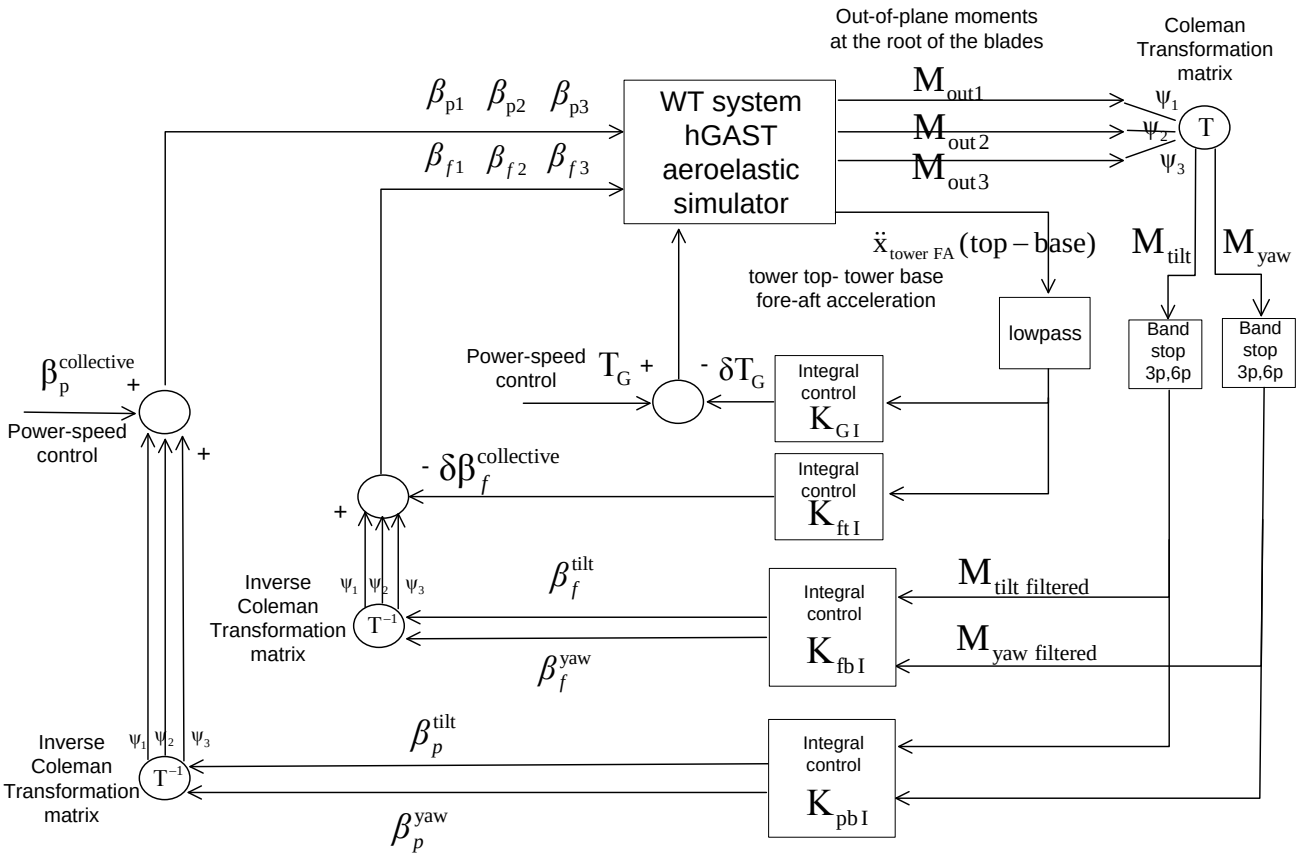

Figure 1: Description of controller.

Table 1: Controller gains for the different control elements.

IPC&IFC	$K_{pbI} = 0.6 \times 10^{-9}$ deg/ s / Nm $K_{fbI} = 5 \times 10^{-9}$ deg/ s / Nm
Generator & Collective flap	$K_{GI} = 1 \times 10^{6}$ Nm / m / s^2 $K_{ftI} = 4 \times 10^{-2}$ deg s / m

Table 2: TE flap layout.

Flap configuration	
	10MW
Chordwise extent	30%
Deflection angle limits	±10°
Deflection speed limit	20°/s
Spanwise length	30 m (~34% of blade length)
Spanwise location	55 m-85 m (from rotor centre)
Airfoil	FFA-W3-241

Table 3: Simulated DLCs.

DLC	Definition	Bins [m/s]	Yaw(deg)
1.2	NTM, NSS	5,9,13,17,21,25	0
1.3	ETM, NSS	11,25	0
1.6	NTM, SSS	11,25	0

Table 4: Definition of sea state.

NSS		
U [m/s]	Hs [m]	Tp [s]
5.0	1.14	5.78
7.0	1.25	5.67
9.0	1.40	5.71
11.0	1.59	5.81
13.0	1.81	5.98
15.0	2.05	6.22
17.0	2.33	6.54
19.0	2.62	6.85
21.0	2.93	7.20
23.0	3.26	7.60
SSS		
	9.40	13.70

Fatigue loads (Table 5)

- Flapwise bending moment DEL decreases by 13.4%. Higher reduction of the flapwise moment DEL is obtained in the wind speeds range 17-21 m/s.
- A slight reduction of 1.4% is also noted on the edgewise bending moment DEL. Higher reduction rates are obtained in the vicinity of the rated wind speed (9 and 13 m/s).
- Blade torsion moment DEL significantly increases (about 60%). The rate of increase is higher at higher wind speeds. The increase in the torsion moment is due to the increase in the twisting moment induced by the moving flaps.
- Tower fore-aft moment decreases by 1.8%. Side-side moment also decreases by 2.9%.
- A marginal increase of 0.3% is noted on the yaw moment DEL
- As a result of the lower tower fatigue loads, reduced DELs are obtained on the mooring lines. An average reduction of about 3% is noted on the fairleads and the anchors.

Ultimate loads (Table 6)

- Extreme (maximum) flapwise bending moment increases by 2.7%. The driving DLC for the flapwise moment is DLC 1.6. So, high flapwise loads are driven by extreme sea conditions. In case of extreme wind turbulence, maximum flapwise moment decreases by 7.8%.
- A 5.9% reduction of the maximum (ultimate load) edgewise bending moment is obtained.
- A 33% maximum torsion moment increase is obtained. This is again due to the twisting moment induced by the moving flaps.
- Overall the combined blade moment increases by 2.7%. The increase in the combined moment is driven by the high (by the same percentage) flapwise bending moment in DLC 1.6.
- Maximum tower fore-aft moment decreases by about 1%.
- Ultimate tower side-side moment decreases by 13.1% and yaw moment decreases by 1.9%
- The overall reduction of the combined tower moment is about 1%. It is seen that combined tower base moment is essentially driven by fore-aft component. The rates of combined tower moment reduction are exactly the same with those of the tower fore-aft moment component.
- A slight reduction of the mooring line loads is noted in most cases.

Table 5: Lifetime DELs calculated for 20 years with Weibull parameters C=11 m/s and k=2, Wöhler coefficient m=4 for the tower and the jacket and m=10 for the blades and $n_{ref}=10^8$ cycles.

			5m/s	9m/s	13m/s	17m/s	21m/s	25m/s	Overall
ROOT BLADE	edge (kNm)	default	21953	23792	24605	24793	25285	26038	23718
		ipc_ifc_gen_flap	-0.6%	-2.4%	-1.5%	-0.6%	0.0%	0.3%	-1.4%
	flap (kNm)	default	5309	12820	24349	24836	28798	32469	23534
		ipc_ifc_gen_flap	-8.8%	-7.6%	-10.4%	-16.1%	-15.9%	-13.4%	-13.4%
	torsion (kNm)	default	290	283	401	406	429	455	371
		ipc_ifc_gen_flap	3.2%	12.6%	36.1%	54.6%	70.5%	83.6%	57.9%
TOWER BASE	side (kNm)	default	4846	21879	41632	59618	74993	92204	44410
		ipc_ifc_gen_flap	3.1%	-0.5%	-4.2%	-2.5%	-2.4%	-3.5%	-2.9%
	fore (kNm)	default	105895	129572	184844	198201	231941	274445	162040
		ipc_ifc_gen_flap	-0.9%	-1.8%	-2.3%	-2.2%	-1.2%	-0.6%	-1.8%
	yaw (kNm)	default	4220	8880	16422	20289	23797	27035	15101
		ipc_ifc_gen_flap	4.8%	-1.5%	-0.5%	0.0%	1.1%	2.1%	0.3%
FAIRLEADS	fairleads1 (kN)	default	51	120	141	121	143	183	119
		ipc_ifc_gen_flap	0.3%	-1.2%	1.2%	-7.0%	-4.8%	-5.2%	-1.2%
	fairleads2 (kN)	default	75	82	97	125	131	146	95
		ipc_ifc_gen_flap	1.3%	1.9%	-4.0%	-7.4%	-2.0%	0.1%	-2.8%
	fairleads3 (kN)	default	52	121	147	118	144	183	121
		ipc_ifc_gen_flap	0.2%	0.7%	-5.7%	-10.1%	-8.3%	-6.0%	-4.1%
ANCHOR	anchor1 (kN)	default	49	114	134	117	140	181	114
		ipc_ifc_gen_flap	-0.1%	-0.9%	1.2%	-6.8%	-4.6%	-5.4%	-1.2%
	anchor2 (kN)	default	67	70	83	111	171	252	102
		ipc_ifc_gen_flap	1.4%	1.5%	-4.4%	-6.8%	-7.1%	-0.6%	-3.3%
	anchor3 (kN)	default	50	116	141	114	140	180	116
		ipc_ifc_gen_flap	0.5%	0.8%	-5.9%	-9.7%	-7.4%	-5.4%	-4.1%

Table 6: Min-max loads – Min and Max loads of the fatigue DLC 1.2 are also included.

			DLC 1-2		DLC 1-3		DLC 1-6		Overall	
			max	min	max	min	max	min	max	min
ROOT BLADE	edge (kNm)	default	23466	-22195	25155	-23643	46365	-24434	46365	-24434
		ipc_ifc_gen_flap	-2.1%	1.4%	-2.3%	0.5%	-5.9%	2.0%	-5.9%	2.0%
	flap (kNm)	default	53779	-23820	63558	-28739	92886	-64930	92886	-64930
		ipc_ifc_gen_flap	-0.5%	-5.7%	-7.8%	-15.4%	2.7%	2.3%	2.7%	2.3%
	torsion (kNm)	default	435	-637	548	-670	1597	-641	1597	-670
		ipc_ifc_gen_flap	77.0%	48.7%	58.1%	50.3%	33.3%	105.6%	33.3%	96.7%
	combined (kNm)	default	55327		66943		93309		93309	
		ipc_ifc_gen_flap	-1.6%		-12.2%		2.7%		2.7%	
TOWER BASE	side (kNm)	default	121412	-78040	137998	-95393	125321	-68494	137998	-95393
		ipc_ifc_gen_flap	-18.8%	-10.4%	-13.1%	-4.9%	-6.2%	0.5%	-13.1%	-4.9%
	fore (kNm)	default	397862	-272383	430593	-299583	891652	-822967	891652	-822967
		ipc_ifc_gen_flap	-2.5%	0.0%	0.2%	2.5%	-0.9%	-6.0%	-0.9%	-6.0%
	yaw (kNm)	default	34990	-37666	37352	-43274	33630	-36122	37352	-43274
		ipc_ifc_gen_flap	-10.2%	-16.0%	-12.6%	-17.1%	8.9%	5.4%	-1.9%	-12.0%
	combined (kNm)	default	402816		430636		891804		891804	
		ipc_ifc_gen_flap	-3.5%		0.3%		-0.9%		-0.9%	
FAIRLEADS	fairleads1 (kN)	default	3903	3015	4106	3049	6498	1876	6498	1876
		ipc_ifc_gen_flap	0.2%	-0.1%	-0.2%	-0.4%	-1.3%	1.2%	-1.3%	1.2%
	fairleads2 (kN)	default	1207	540	1172	359	1456	7	1456	7
		ipc_ifc_gen_flap	0.2%	-0.5%	-1.0%	-5.8%	-2.7%	13.9%	-2.7%	13.9%
	fairleads3 (kN)	default	3911	2966	4118	2938	6433	1793	6433	1793
		ipc_ifc_gen_flap	-0.2%	1.3%	-0.8%	4.0%	-0.4%	2.8%	-0.4%	2.8%
ANCHOR	anchor1 (kN)	default	3405	2569	3597	2593	6017	942	6017	942
		ipc_ifc_gen_flap	0.2%	-0.1%	-0.2%	-0.6%	-1.6%	7.3%	-1.6%	7.3%
	anchor2 (kN)	default	930	143	934	157	2154	0	2154	0
		ipc_ifc_gen_flap	-0.3%	-14.2%	-0.5%	-1.2%	1.7%	21.5%	1.7%	21.5%
	anchor3 (kN)	default	3415	2516	3610	2492	5957	857	5957	857
		ipc_ifc_gen_flap	-0.2%	1.7%	-1.0%	4.4%	-0.7%	4.6%	-0.7%	4.6%

In Figure 2 and Figure 3 the flap and pitch motion characteristics of the controller are presented for the NTM conditions. It is seen that the flap motion reaches the saturation limit of +/-10^o at wind speeds higher than 13m/s (see Figure 2). The SDV of the flap angle is significantly lower than the limit angle of 10^o (goes up to 5^o) indicating that flap motion stays well below the limit angles most of the time and occasionally hits the upper bound.

In Figure 3 the SDV of the pitch motion is shown for the baseline controller in comparison to the advanced controller. It is seen that the increase of the SDV of the pitch motion is less than 10% at all wind speeds in the full loads region.

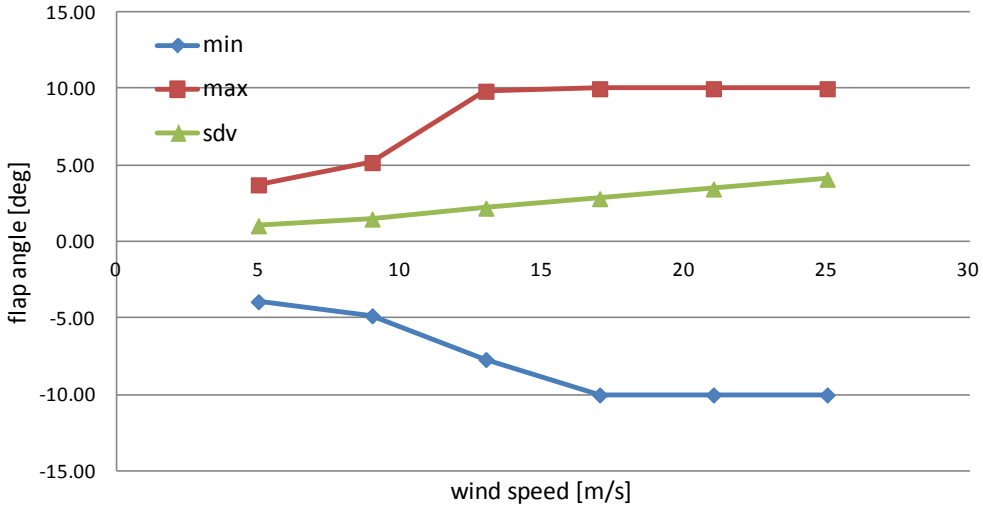

Figure 2: Flap angle variation.

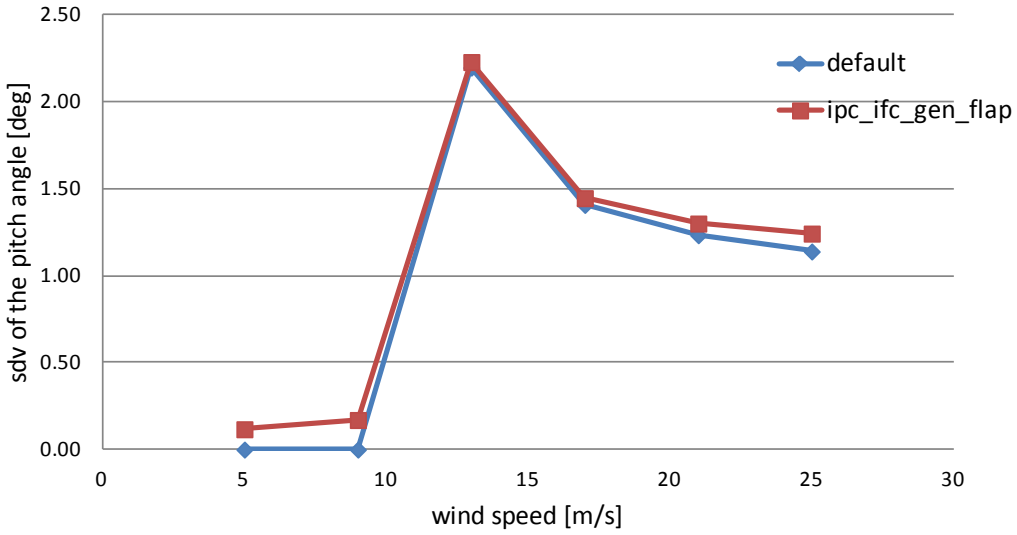

Figure 3: Pitch angle variation.

3.0 Evaluation of 10 MW 2 Bladed Semi Floater with Optimized Blades (DTU)

In this work, an optimized blade design for a 10 MW two-bladed downwind turbine is evaluated in terms of ultimate and fatigue loads for a Semi Floater solution. In [**5**], three optimized blade designs were considered to assess increasing AEP, to ensure tower clearance issues and to maintain loads within the same load envelope as the baseline model. That study revealed the configuration with blade R1.08 (optimally stretched by 8% length) and 2.5° pre-cone as a feasible solution which met the aforementioned criteria. The R1.08 blades resulted in a mass reduction of ≈11% and an increased AEP of 8% (onshore setup). In the following work, the blade R1.08 is implemented for a 10 MW two-bladed downwind turbine mounted on a Semi Floater, which was previously designed and evaluated in [**6**]. The loads of the newly implemented R1.08 blades are compared with the baseline model of downwind 10 MW two-bladed [**7**] and the baseline equipped with Individual Flap Control (IFC). The baseline model and baseline with IFC are evaluated in [**8**].

3.1 Design loads and sensors

The design load cases considered are based on the IEC 61400-3. DLC 1.2 is assessed for fatigue analysis; DLC 1.3 and 6.2 for the ultimate load analysis. The metocean conditions are presented in [**9**].

DLC 1.2: 12 wind speeds (4 - 26 m/s with 2 m/s step) with yaw errors ±10° and wind-wave misalignment of ±10° are applied. Six seeds per scenario are considered. Overall 648 simulations are run.

DLC 1.3: 12 wind speeds (4 - 26 m/s with 2 m/s step) with yaw errors ±10°. Two seeds per scenario are considered. Wind and wave are aligned. Overall 72 simulations are run.

DLC 6.2: 24 load directions are simulated (with 15° step) at 42.73 m/s. Three seeds per scenario are considered with no yaw misalignment. Wind and wave are aligned. Overall 72 simulations are run. Table 3 introduces the load channels evaluated in the present study.

The fatigue loads are given as a damage equivalent load of 10^7 cycles, Nref, corresponding to 25 years life time damage

Table 7: load channels

Load channels		Wholer exponent m
MxTB	Tower bottom fore-aft	4
MyTB	Tower bottom side-side	4
MxTT	Tower top tilt	4
MyTT	Tower top roll	4
MzTT	Tower top yaw	4
MxMB	Main bearing tilt	4
MyMB	Main bearing yaw	4
MzMB	Main bearing torsion	4
MxBR	Blade root flap	4
MyBR	Blade root edge	4
MzBR	Blade root torsion	4
MxFB	Foundation moment fore-aft	4
MyFB	Foundation moment side-side	4
MzFB	Foundation moment torsion	4
MxFT	Floater base moment fore-aft	4
MyFT	Floater base moment side-side	4
MzFT	Floater base moment torsion	4
FxML	Axial force in mooring line	4

3.2 Power Curve

The power curve displayed in Figure 4 is computed as the mean value over simulations from DLC1.2. For the assumed metocean conditions of DLC1.2, the optimized rotor produces 3.4% higher AEP compared to the baseline model.

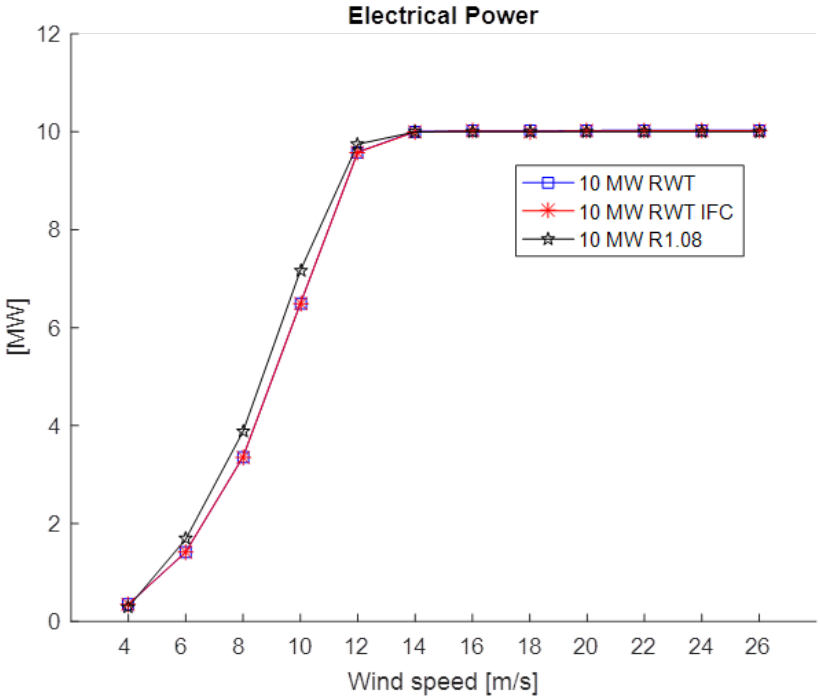

Figure 4: Power curve - 10 MW RWT, 10 MW RWT IFC and 10 MW R1.08

3.3 Ultimate limit state

The ultimate loads are computed based on DLC 1.3 and 6.2. Figure 5 shows the resulting ultimate loads for the optimized rotor (*10 MW R1.08)* and the baseline with IFC (*10 MW RWT IFC)* normalized on the baseline model (*10 MW RWT*). It is found that the optimized rotor achieves ultimate load reduction for flapwise root bending moment of 22%. Besides, improved ultimate loads are observed for tower top tilt (27% compared to baseline) and (12% compared to IFC setup), and for shaft tilt bending (23% compared to baseline). A significant increase of the shaft yaw bending moment (MyMB) is found for the optimized rotor (≈62%). Higher ultimate MyMB were also observed for the optimized rotor in the onshore configuration evaluated in D2.14. Eventually, the optimized rotor configuration delivers slightly improved ultimate loads at the Semi Floater structure, where the tower base fore-aft moment is reduced by 3%, the floater base fore-aft by 3.5% and floater base side-side by 6%, the joint top fore-aft by 3%. Table 8 summarizes the ultimate loads at tower top, at the interface between tower-semi floater and at the joint top.

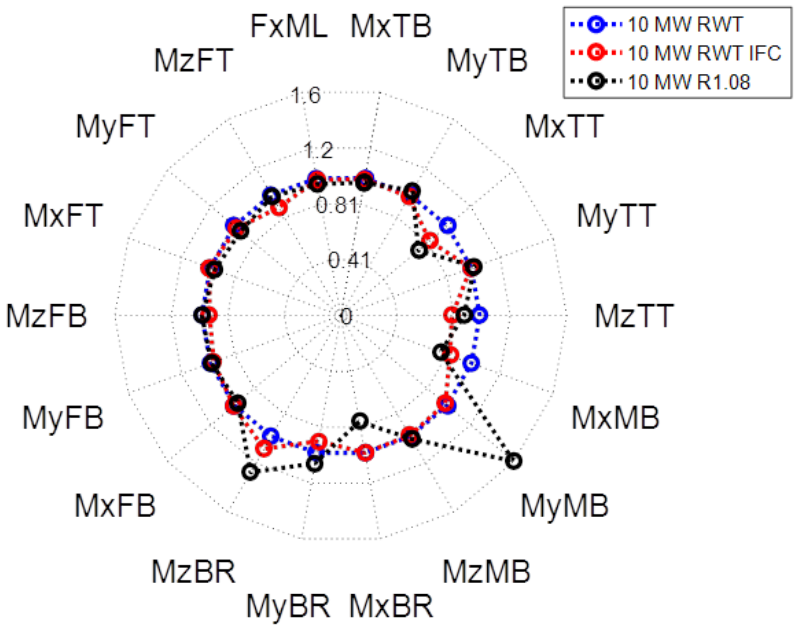

Figure 5: Comparison of ultimate loads – 10 MW RWT, 10 MW RWT IFC and 10 MW R1.08

Table 8: Ultimate loads for tower top interface and Joint top – 10 MW RWT, 10 MW RWT IFC and 10 MW R1.08

Tower Top	MxTT [kNm]	MyTT [kNm]	MzTT [kNm]
10 MW RWT	130909	17093	28202
10 MW RWT + IFC	109179	17032	22549
10 MW R1.08	95437	17518	24981
Interface	MxTB [kNm]	MyTB [kNm]	MzTB [kNm]
10 MW RWT	315044	166255	28273
10 MW RWT + IFC	312776	163496	23929
10 MW R1.08	305581	172114	24589
Joint Top	MxFB [kNm]	MyFB [kNm]	MzFB [kNm]
10 MW RWT	512810	288767	0.461
10 MW RWT + IFC	516739	280920	0.435
10 MW R1.08	496670	286279	0.460

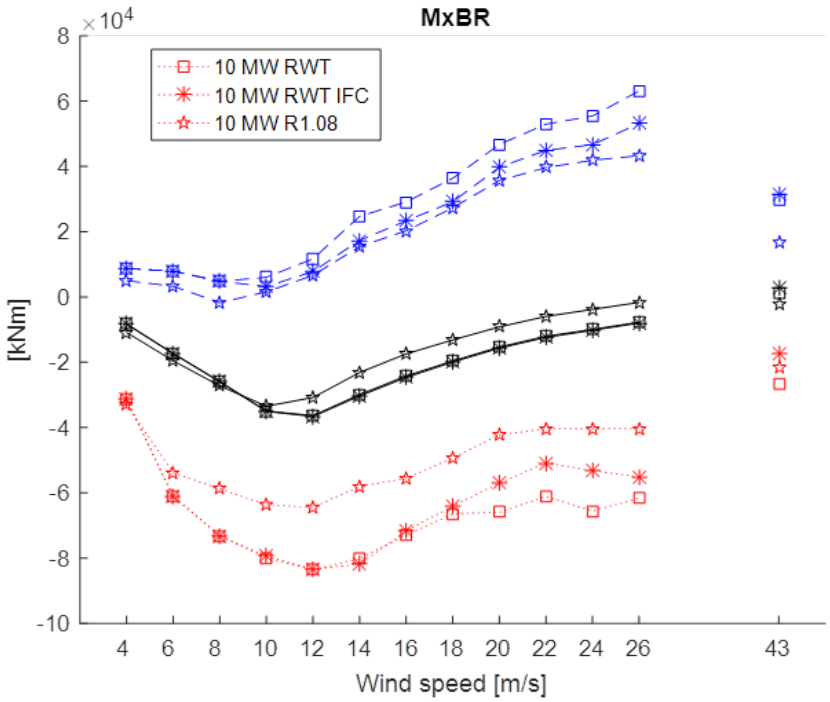

Figure 6: Ultimate loads for MxBR - 10 MW RWT, 10 MW RWT IFC and 10 MW R1.08

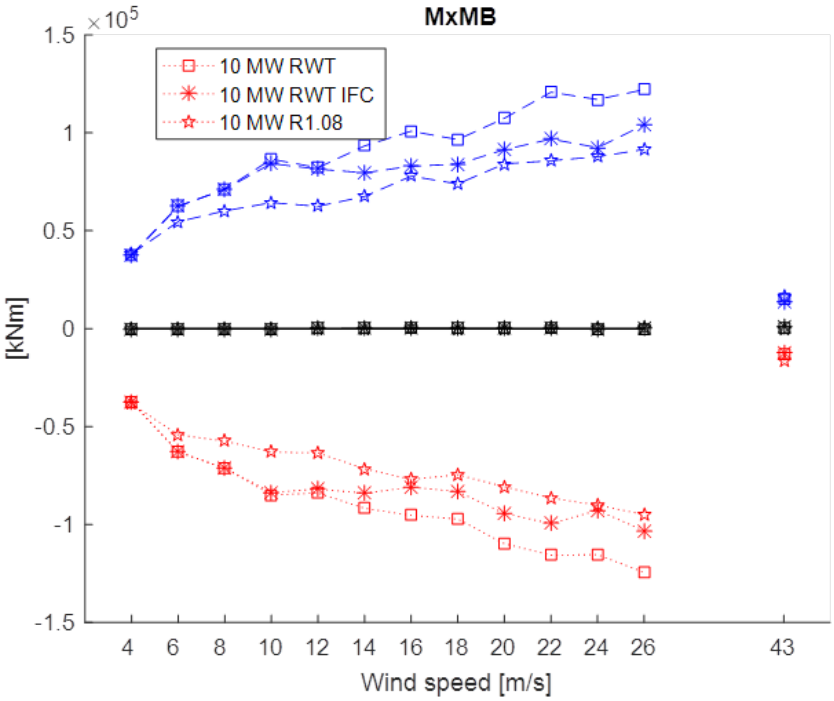

Figure 7: Ultimate loads for MxMB - 10 MW RWT, 10 MW RWT IFC and 10 MW R1.08

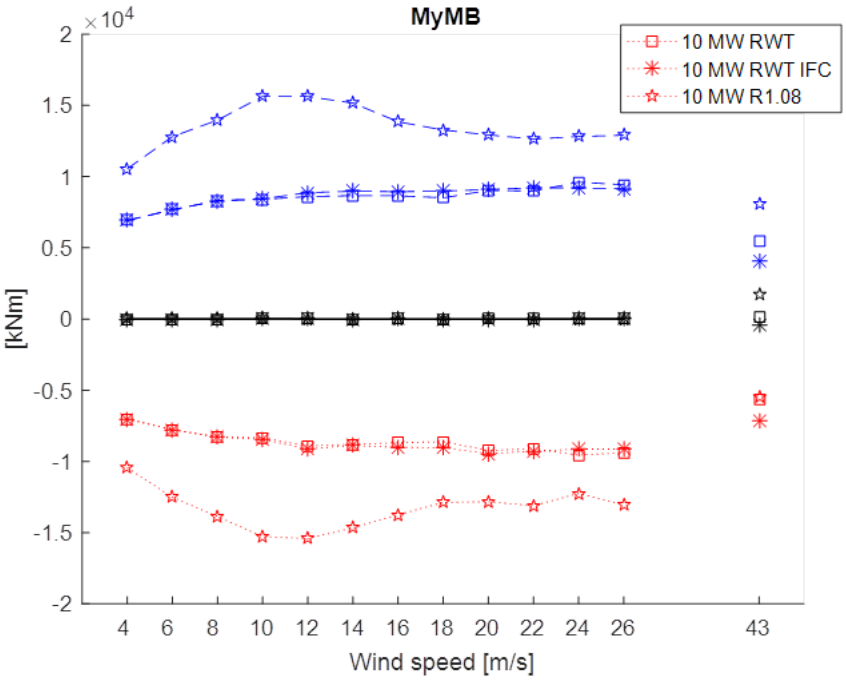

Figure 8: Ultimate loads for MyMB - 10 MW RWT, 10 MW RWT IFC and 10 MW R1.08

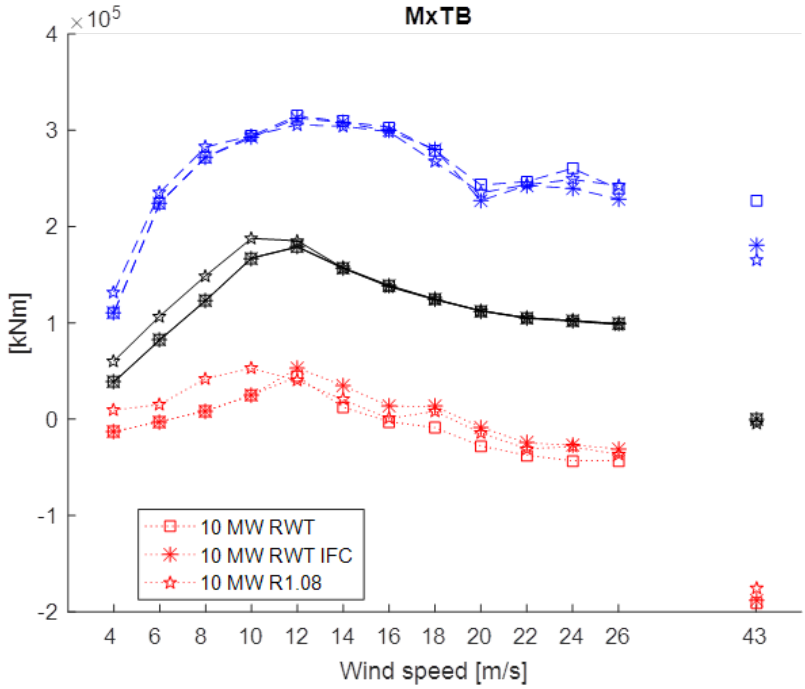

Figure 9: Ultimate loads for MxTB - 10 MW RWT, 10 MW RWT IFC and 10 MW R1.08

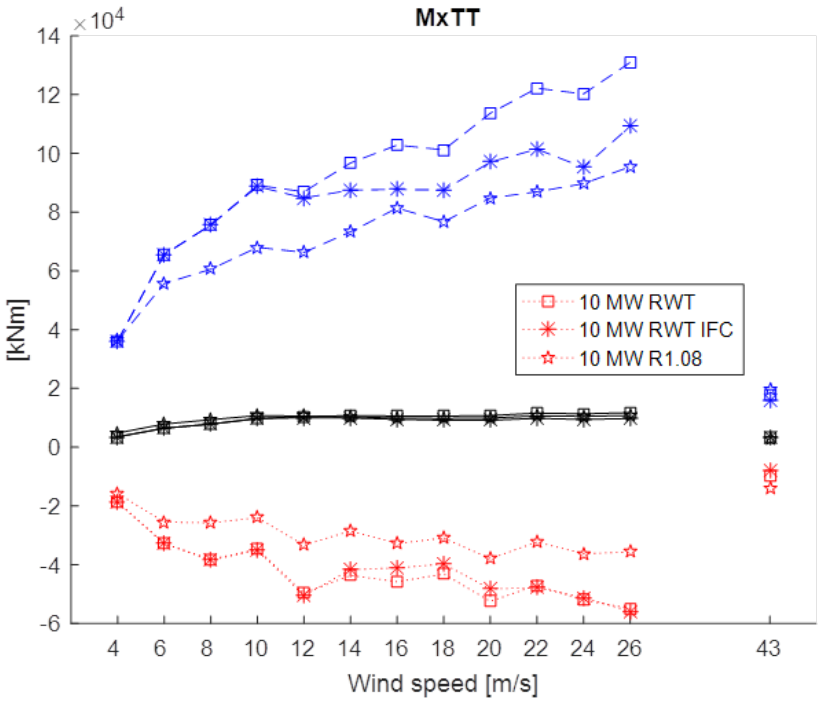

Figure 10: Ultimate loads for MxTT - 10 MW RWT, 10 MW RWT IFC and 10 MW R1.08

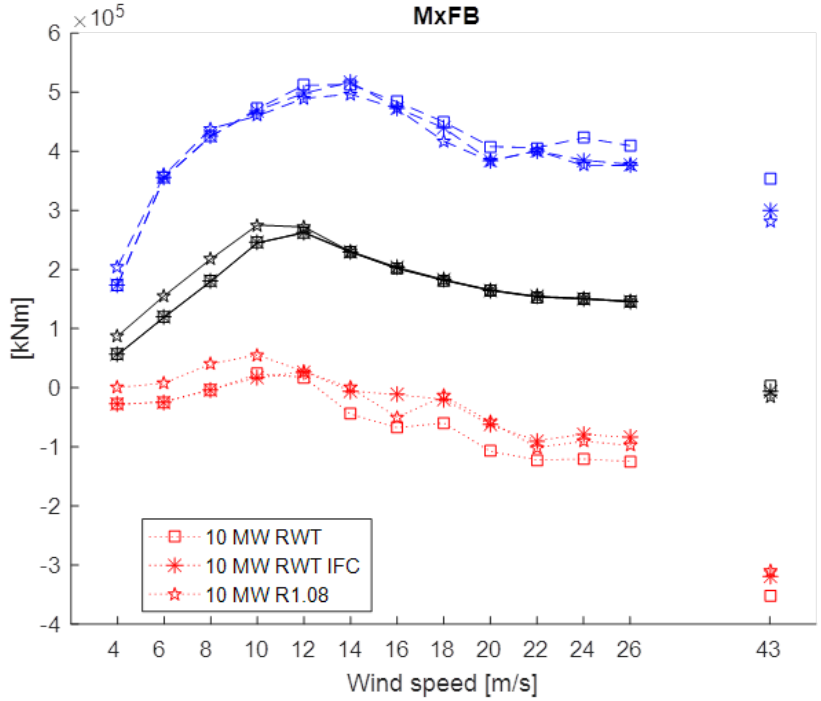

Figure 11: Ultimate loads for MxFB - 10 MW RWT, 10 MW RWT IFC and 10 MW R1.08

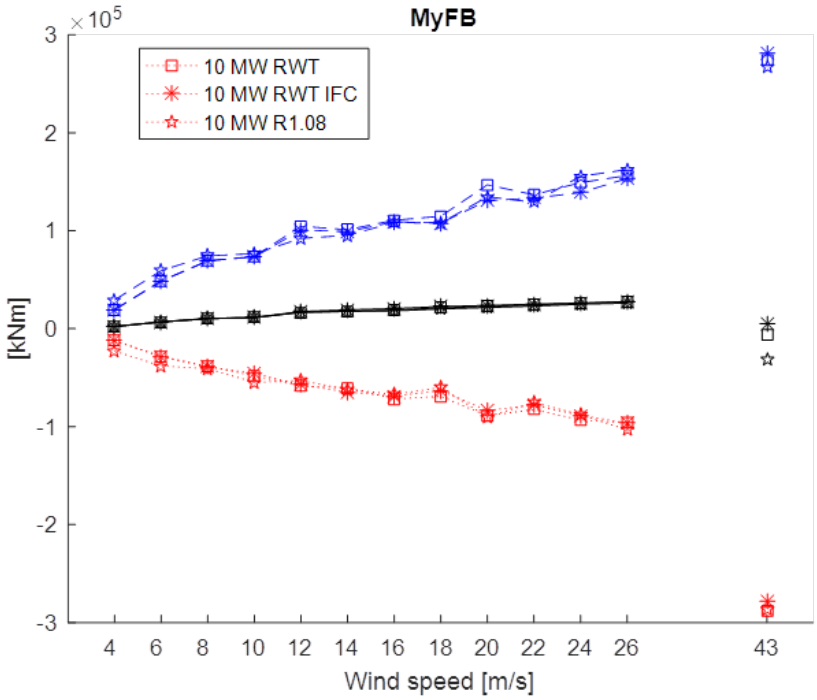

Figure 12: Ultimate loads for MyFB - 10 MW RWT, 10 MW RWT IFC and 10 MW R1.08

3.4 Fatigue limit state

Figure 13 shows the lifetime fatigue loads for the "*10 MW R1.08*" and "*10 MW RWT IFC*" normalized on the baseline model "*10 MW RWT*". Overall both the optimized rotor and the setup with IFC deliver reduced fatigue loads in comparison to the baseline model. The two setups achieve reduced flapwise root moment; around 33% lower loads are demonstrated for the optimized rotor. Despite a noticeable increase of the shaft yaw bending moment of 27%, the optimized rotor delivers improved loads for both tower top and tower base (at the interface with the semi floater). This resulted in lower fatigue loads computed at the semi floater structure, where reduction of 19% (compared to baseline) and 4% (compared to IFC setup) is achieved at the joint top for-aft bending moment. Besides, reduced fatigue loads at floater base fore-aft; side-side and torsion of respectively 19%, 6% and 16% are observed for of the optimized rotor compared to baseline. Table 9 summarizes the lifetime fatigue loads for the tower top, interface between tower and semi floater and joint top.

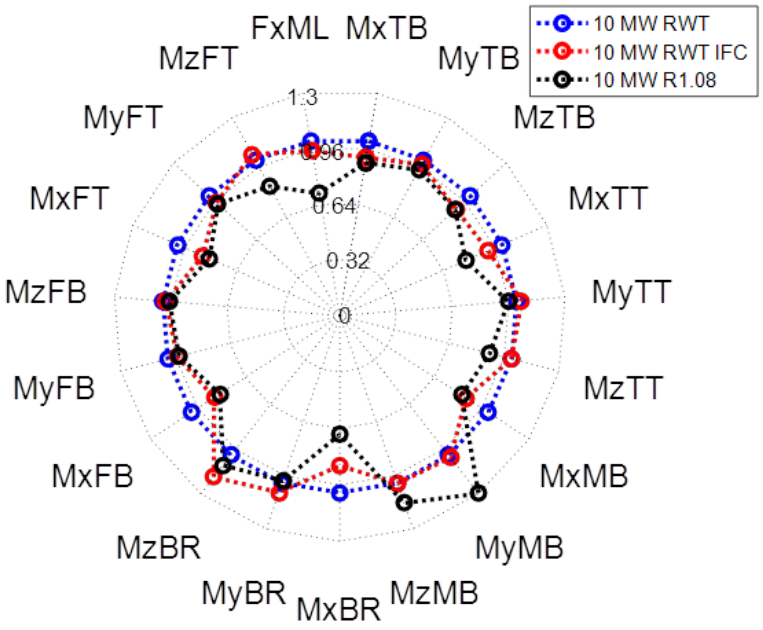

Figure 13: Comparison of lifetime fatigue loads - – 10 MW RWT, 10 MW RWT IFC and 10 MW R1.08

Table 9: Lifetime fatigue loads for tower top interface and Joint top – 10 MW RWT, 10 MW RWT IFC and 10 MW R1.08

Tower Top	MxTT [kNm]	MyTT [kNm]	MzTT [kNm]
10 MW RWT	788350	2739	14303
10 MW RWT + IFC	72003	2818	14275
10 MW R1.08	61191	2611	12476
Interface	MxTB [kNm]	MyTB [kNm]	MzTB [kNm]
10 MW RWT	116460	55107	13891
10 MW RWT + IFC	105565	53521	12356
10 MW R1.08	102128	51626	12283
Joint Top	MxFB [kNm]	MyFB [kNm]	MzFB [kNm]
10 MW RWT	221956	95462	0.114
10 MW RWT + IFC	187787	90194	0.112
10 MW R1.08	179309	89179	0.110

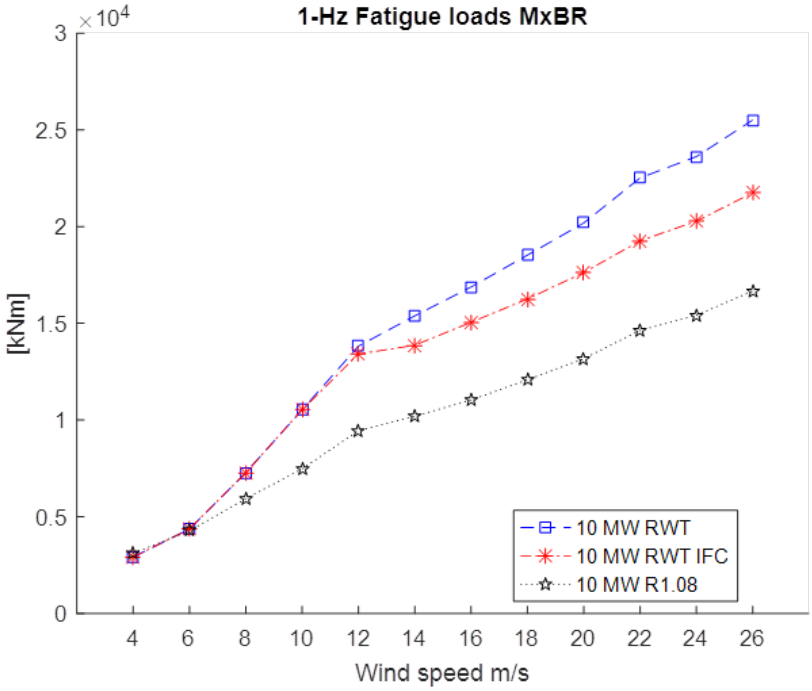

Figure 14: 1-Hz fatigue load - MxBR

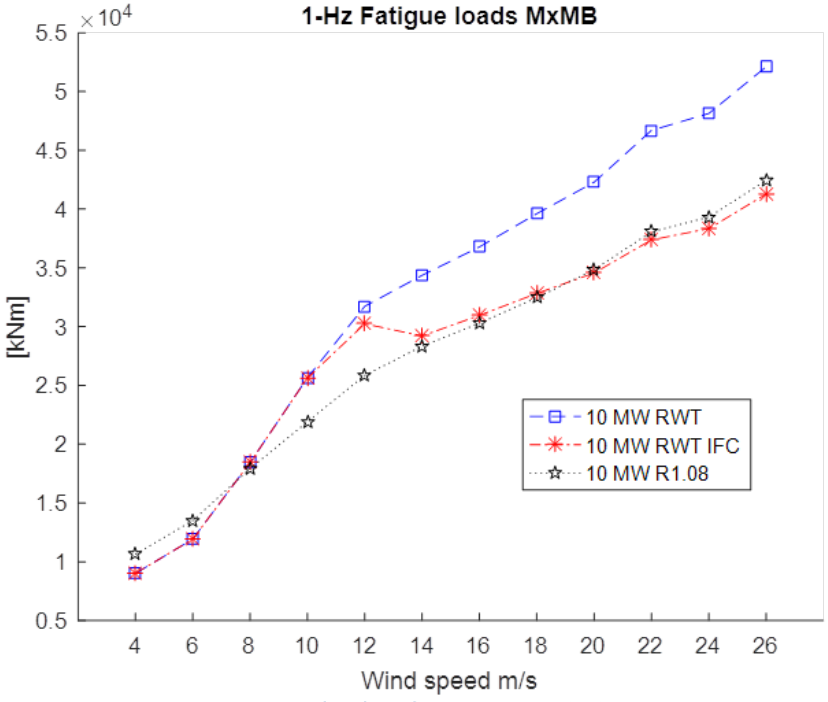

Figure 15: 1-Hz fatigue load – MxMB

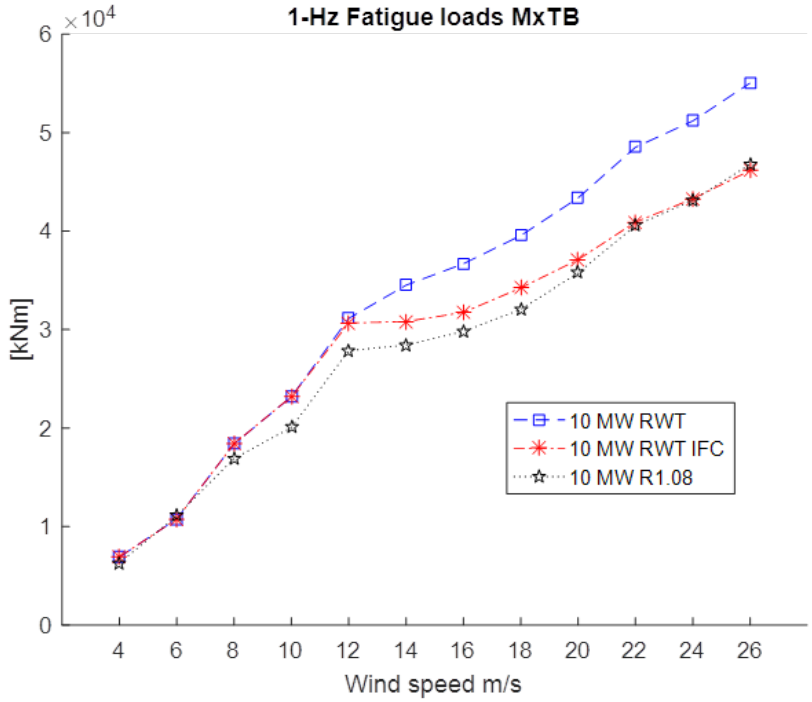

Figure 16: 1-Hz fatigue load - MxTB

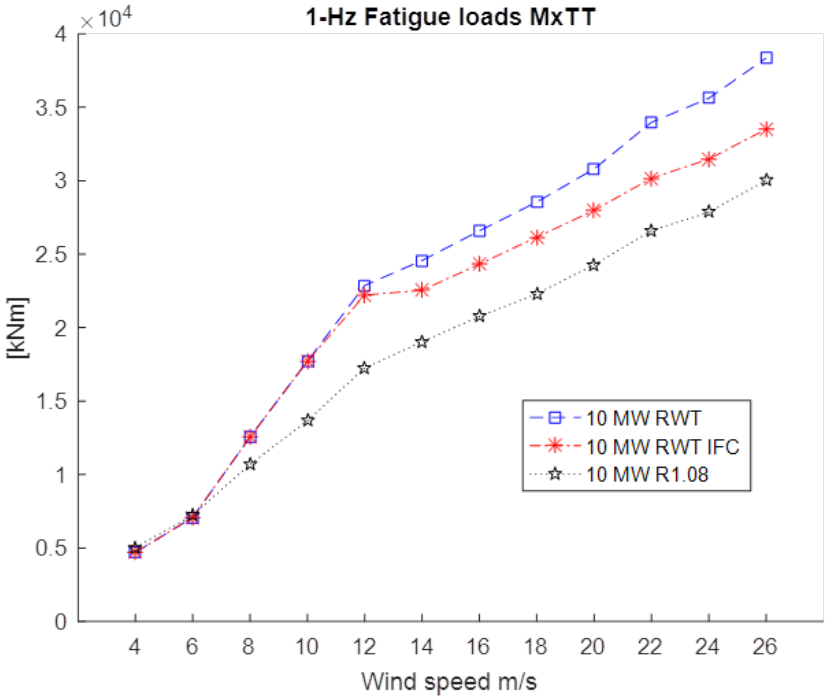

Figure 17: 1-Hz fatigue load – MxTT

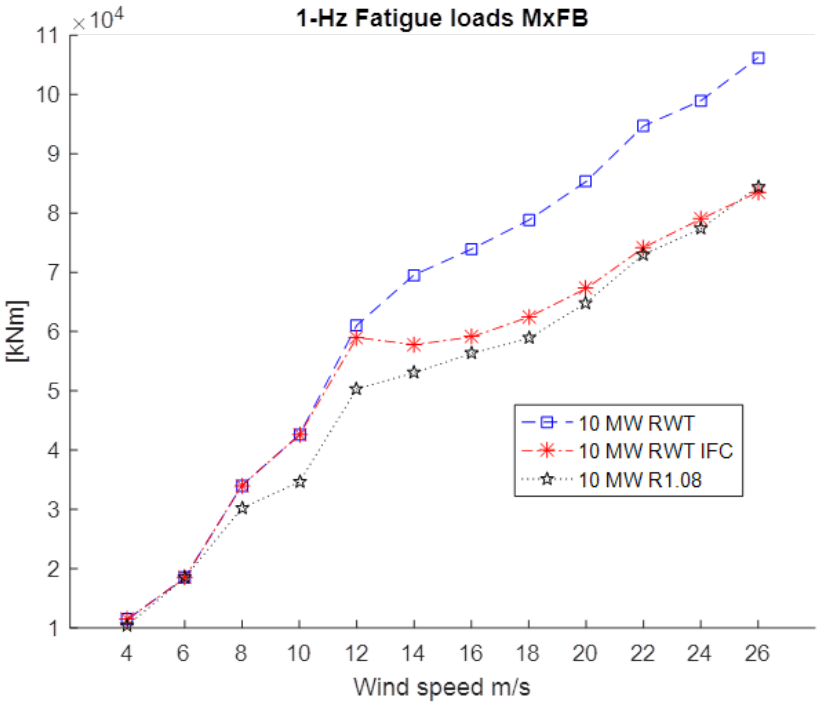

Figure 18: 1-Hz fatigue load - MxFB

3.5 Discussion

The ultimate and fatigue loads analysis is evaluated for the 2-bladed downwind 10 MW RWT on Semi Floater including Individual Flap Control and an Optimized rotor design. The optimized blade R1.08 was designed in D2.14 and resulted in an optimally stretched 8% longer blade with 2.5° pre-cone. An assessment of the AEP for the offshore Semi Floater application shows an increase of 3.4%. Regarding the lifetime fatigue loads, the optimized rotor achieves reduced tower base loads (fore-aft 12% and side-side 6.3%), resulting in improved fatigue life of the Semi Floater structure. Thus, fatigue loads computed at the floater base, including fore-aft; side-side bending moments and torsion are found respectively 19%, 6% and 16% lower for the optimized rotor. Moreover, reduced fatigue loads of 19% (compared to baseline) and 4% (compared to IFC setup) is achieved at the joint top for-aft bending moment. Oppositely, a large increase of the lifetime fatigue yaw bending moment at the shaft of 27% is observed for the optimized rotor. Similar results for the main bearing fatigue loads were found in D2.14 for the onshore application. The ultimate load analysis also shows a potential reduction of ultimate loads at Semi Floater structure of ≈ 3% for the tower base fore-aft, floater base fore-aft and joint top fore-aft bending moments. Floater base side-side bending moments are reduced by 6%. Despite a large increase of the shaft-yaw bending moment (≈62%), the optimized rotor achieves significant lower ultimate loads for the flapwise root (22%), tower top tilt (27%) and shaft tilt (23%).

4.0 Evaluation of 20 MW on Jacket with Flap control (GL-GH, now DNV GL (UK))

In this section, we perform an analysis of the additional extreme load reduction capability when using individual flap control in addition to individual pitch control (IFPC) as compared to individual pitch control alone (IPC).

A block diagram of the IFPC controller is shown in Figure 19, with the IP controller losing the IFC labelled blocks. This implementation is makes use of the d-q axis transform (also referred to as the multi-blade coordinate transformation and Coleman transformation) [**10**]. In this structure, each blade is pitched cyclically as a function of azimuth angle, with amplitude defined as a function of the blade root loading. This structure decouples the individual pitch activity from collective pitch activity; which in turn limits impacts on power control and collective pitch damping loops such as tower dampers. The structure also allows the targeting of blade damage at rotor speed harmonic frequencies which account for a significant portion of the blade fatigue loading [**11**]. For this investigation, two harmonics are targeted, 1P and 2P, as they account for most damage accumulation. However, higher order transforms are possible to apply in principle and may be very suitable for application to TEF actuators which can deploy very quickly.

The collective pitch controller (CPC) that operates in parallel with the IPC/IFPC controllers is composed of a speed control loop of proportional-integral (PI) form, and a tower damping control loop of integral form. More detail about the structure can be seen in [**12**], however all controllers have been retuned specifically for this study. For a full explanation of the supervisory control logic used for this investigation, the reader is referred to [**8**].

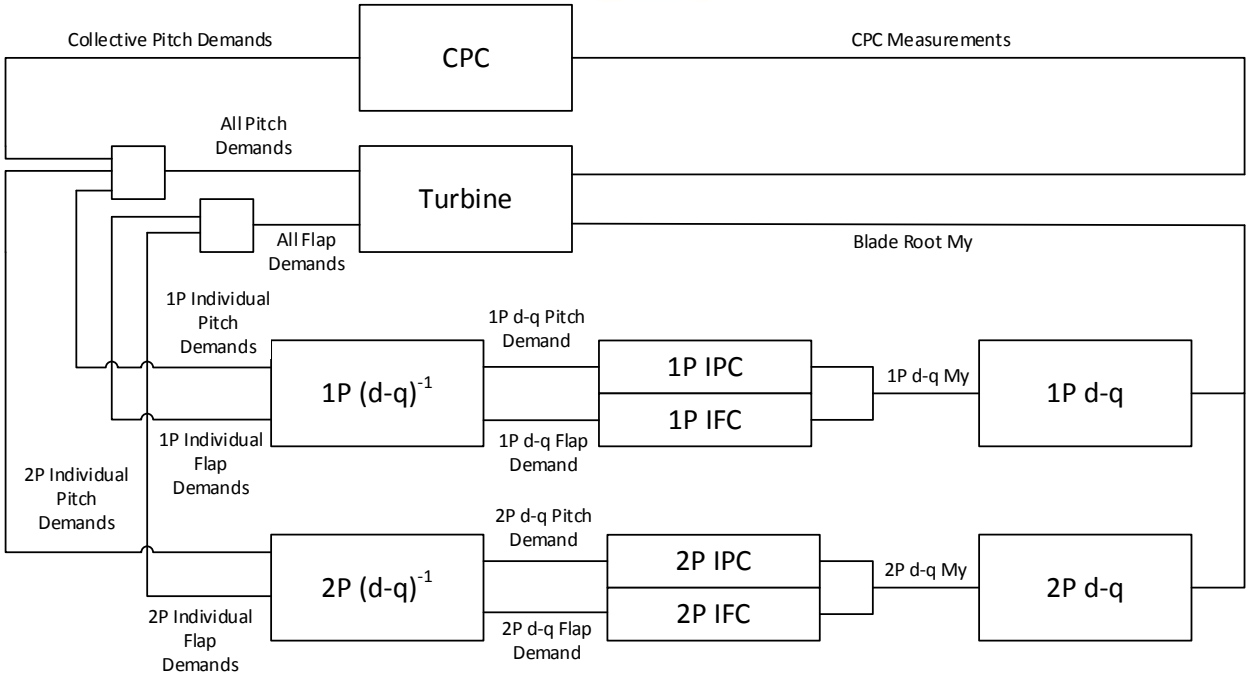

Figure 19: Schematic of IPC and IFC control loops

4.1 Modelling of the 20 MW Reference Turbine with Flaps

4.1.1 Simulation and Analysis Tools

Investigations have been conducted using Bladed 4.8, a validated multi-body wind turbine simulation code. Bladed 4.8 uses blade element and momentum theory to model blade aerodynamics, with the Øye dynamic wake model, the Glauert skew wake model and the Incompressible Beddoes-Leishman dynamic stall model. Flaps are defined as changes to the lift, drag and moment curves, as a function of flap deployment angle for the blade stations containing the active flap. Flap deployment can also be defined with linear dynamics from flap angle demand to flap angle position.

As indicated in [**13**], Bladed does not consider unsteady flow over the flap sections, but the assumption has been made that the frequency of actuation is low enough that unsteady effects do not dominate the response. The reader is referred to [**13**] for a more complete review of the flap modelling performance of a range of engineering codes against CFD models. In that report it was concluded that the results by Bladed acceptable for analysing load reduction potential or active flaps.

4.1.2 Reference 20 MW

The turbine is modelled based on data supplied in [**14**] for the turbine and [**9**] for the advanced steel jacket. The structural model is approximated with:

- 10 modes on each blade;
- 15 support structure modes;
- one drivetrain flexibility; and
- constrained linear actuator dynamics.

A Campbell diagram of the aero-elastically coupled modes is given in Figure 20.

The characteristics of the trailing-edge flap model used for this study are summarised in Table 10

Table 10: Flap configuration for 20 MW Reference Turbine

Flap configuration	
Chordwise extension	30%
Deflection angle limits	$\pm 10^{o}$
Spanwise length	10 m
Spanwise location	105.20 m – 120.02 m (from blade root)
Airfoil	FFA-W3-241
Deflection rate limit	100^{o}/s
Actuator time constant	0.1 s

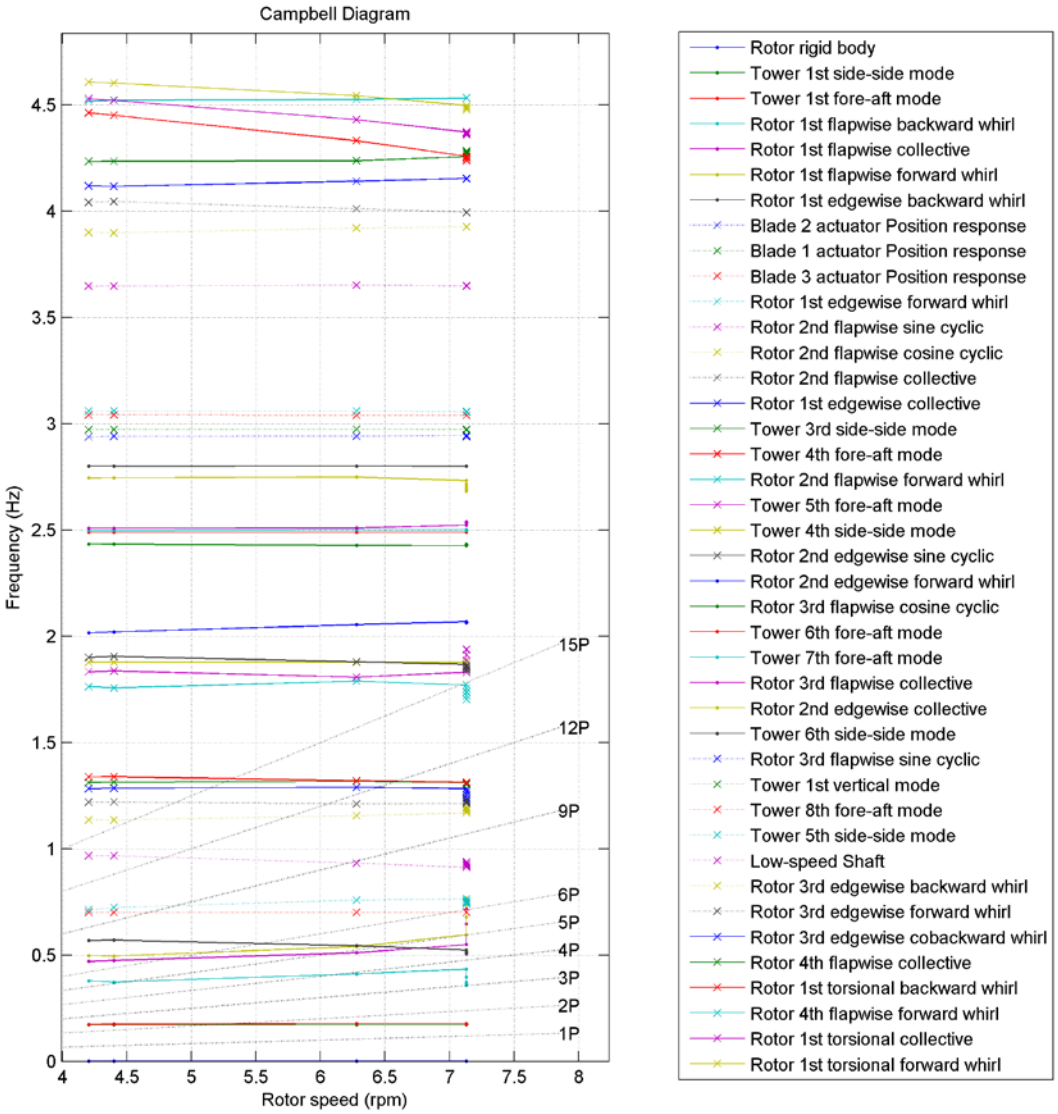

Figure 20: Campbell Diagram for 20 MW Reference Turbine

Coordinate systems

The co-ordinate systems used in this investigation are shown in Figure 21 to Figure 22 below.

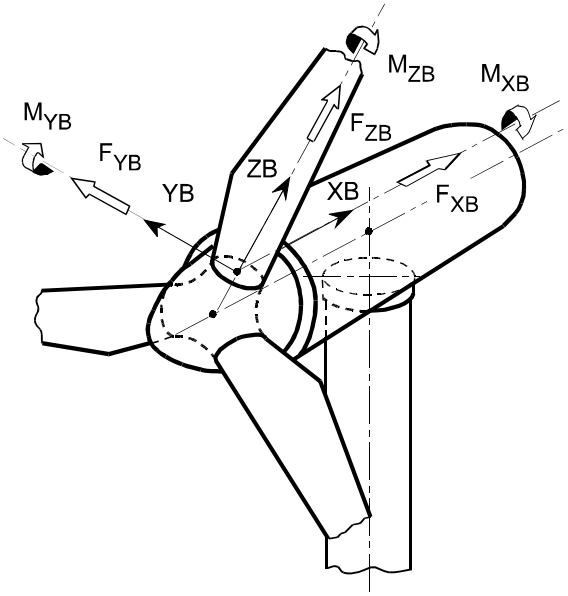

Figure 21: Co-ordinate system for blade root loads and deflections

ZB Radially along blade pitch axis.

XB Perpendicular to ZB, and pointing towards the tower for an upwind turbine, or away from the tower for a downwind turbine (the picture shows an upwind turbine).

YB Perpendicular to blade axis and shaft axis, to give a right-handed co-ordinate system independent of direction of rotation and rotor location upwind or downwind of

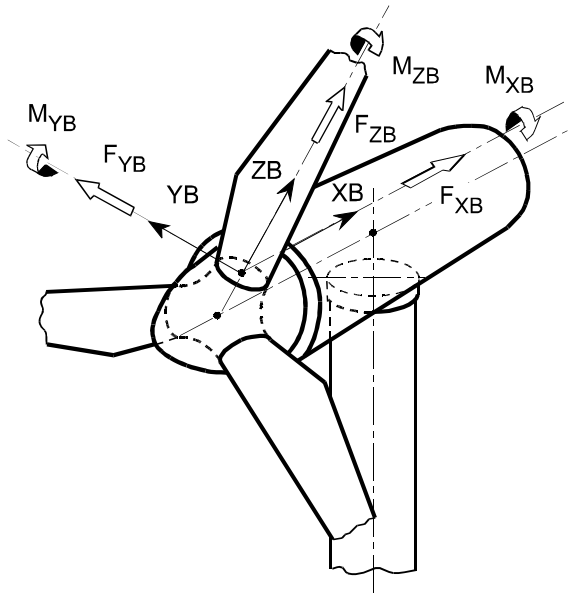

Figure 22: Co-ordinate system for hub loads

Hub loads in fixed frame of reference:

XN Along shaft axis, and pointing towards the tower for an upwind turbine or away from the tower for a downwind turbine.

ZN Perpendicular to XN, such that ZN would be vertically upwards if the tilt angle were zero.

YN Horizontal, to give a right-handed co-ordinate system independent of direction of rotation and rotor location upwind or downwind of the tower.

Origin At hub centre (intersection of blade and shaft axes).

The tower member loads are output with reference to a local member coordinate system for each member. The member x-axis is always aligned along the member. The member z-axis is perpendicular to the member x-axis and aligned according to the direction cosines for the member z-axis as specified in the tower screen of the Bladed interface. These are the direction cosines of the z-axis relative to the global GL coordinate system. The default orientation in Bladed is to set the local member y-axis in the horizontal plane, with the local member z-axis making up a right-handed coordinate system. For a vertical member the default orientation is for the local y-axis to be in the global x-direction, with the local z-axis in the global y-direction. The Bladed output convention for a member situated in the local x-y plane is described in Figure 23 and for a member situated in the local x-z plane in Figure 24.

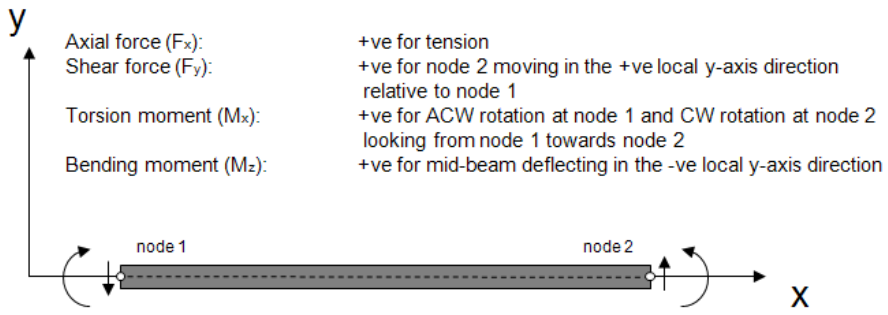

Figure 23: Bladed multi-member output convention: local x-y plane.

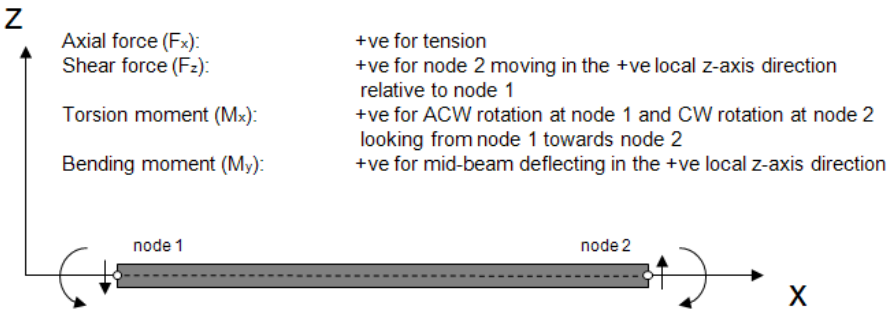

Figure 24: Bladed multi-member output convention: local x-z plane

Locations of key support structure loading outputs are given in Figure 25.

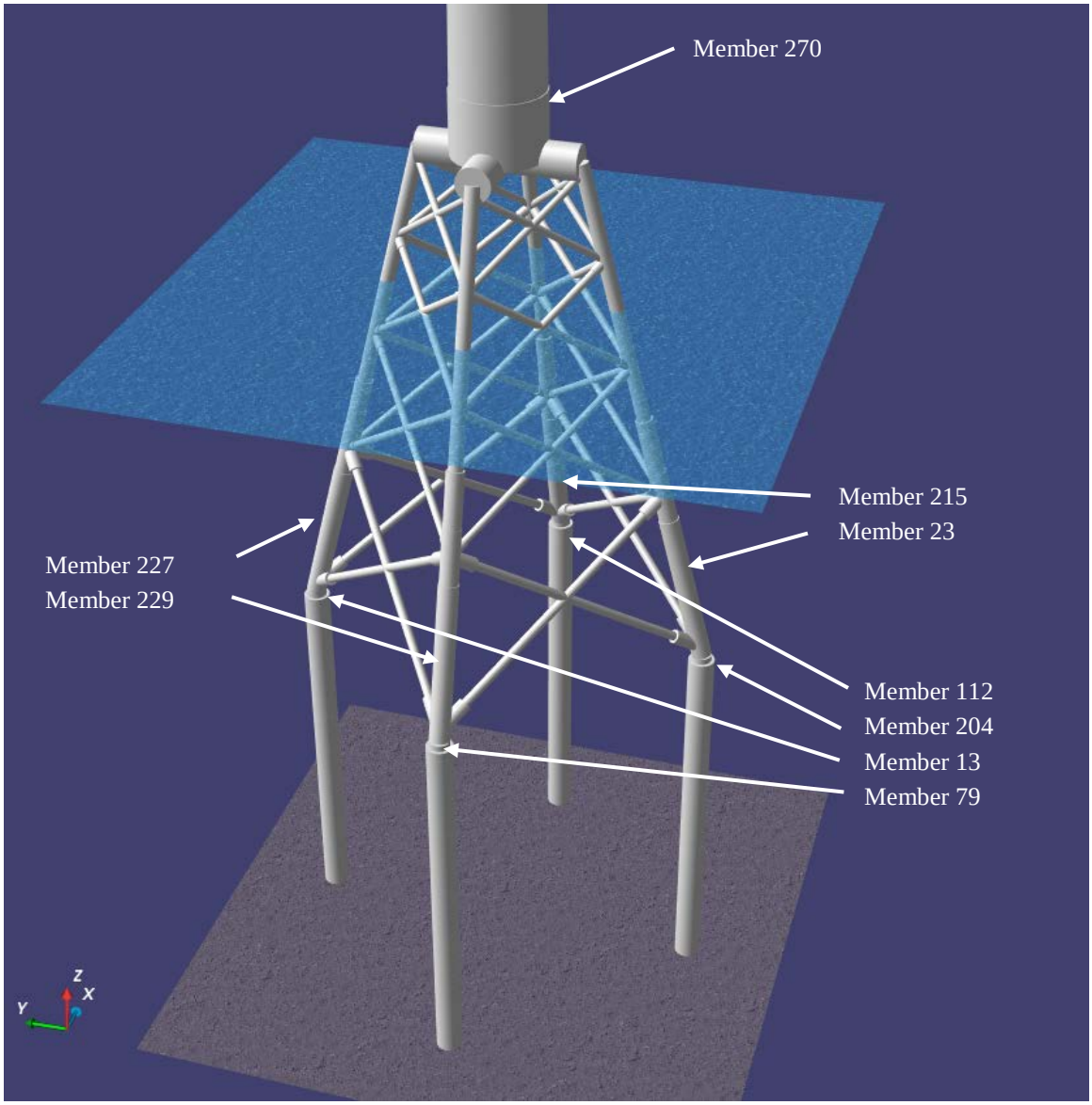

Figure 25: Tower member locations for loads outputs

4.2 Results

As in previous work [**8**], the IFPC controller is designed to deliver the same fatigue loading as an IPC controller. The loading benefits are then derived from the reduction of extreme loads. Design loads are determined through a range of IEC design load cases (DLCs) for Class IC wind conditions [**15**], [**16**], the load cases considered are summarised in Table 11, for a full definition of each load case, the reader is referred to Appendix A Load case definition for 20 MW Reference Turbine.

Table 11: Summary of design loads cases (DLCs)

DLC	Case Type
1.2	Fatigue
1.3	Extreme
1.4	Extreme
2.1	Extreme
2.2	Extreme
2.3	Extreme
2.4	Fatigue
4.1	Fatigue
4.2	Extreme
6.4	Fatigue

Fatigue load calculations have been run with 4 wind directions, and results have been extrapolated to 12 wind directions assuming a constant directional probability. In this case then, loading across the tower corner members and mudline members (see Figure 25) are combined to give the fatigue loading in a single corner member and mudline member. The differences in lifetime damage equivalent loads (DELs) between the IPC and IFPC controllers are given in Table 12. The table shows that both controllers achieve almost identical fatigue load results, with difference below 1%.

Table 12: Difference in lifetime weighted fatigue DELs between IPC and IFPC controllers.

	Mx [kNm]	My [kNm]	Mz [kNm]	Fx [kN]	Fy [kN]	Fz [kN]
Stationary Hub (m= 4)	0.01%	0.00%	0.01%	0.03%	0.10%	0.04%
Blade Root (m= 4)	0.10%	0.00%	0.00%	0.00%	0.03%	-0.15%
Blade Root (m= 4)	0.01%	0.00%	0.00%	0.00%	0.07%	0.20%
Tower Base (m= 4)	0.01%	0.00%	0.00%	0.00%	0.00%	0.00%
Mudline (m= 4)	0.00%	1.00%	0.00%	0.00%	0.00%	0.00%
Brace (m= 4)	0.00%	0.00%	0.00%	0.00%	0.00%	0.00%

Extreme loads for key components are given in Table 13 through Table 23. Note that both the maximum and minimum loads are given, however, it is the maximum load between these two that is taken for any comparative analysis. Key findings can be summarized as:

- Stationary hub loads are largely driven by DLC 1.4 (Extreme coherent gust with direction change), except for the Mx load which is driven by DLC 1.3 (Extreme turbulence). We can see the loads between the two controllers are mostly within 1.5% of each other, however the load targeted by IFPC (Hub Mz = Rotor yaw) has been reduced by 4%.

- Tower base loads (at the transition piece) are again dominated by DLC 1.4 except for the largest Fx load (axial), which is driven by DLC 2.2 algorithm failure and DLC 2.2 n4 overspeed case. Tower base torsional loads (Mx) have reduced 4.37% when using flap control. The maximum resolved overturning moment (Myz) which has been reduced by 1.52% by using flaps. The maximum resolved overturning moment (Fyz) has reduced by 0.51%% while using flaps. Flap control has then reduced overall extreme loading on the tower base.

- Blade root loads are driven by DLC 1.4. Apart from edgewise moments, shear forces and axial forces, adding flaps reduces blade root extreme loading. The key reductions are seen in flap directions (My, Fx) with thrust moments reducing 3.05% and thrust shear forces reducing between 2.28 and 3.62%.

- At the mud line, loads are driven by DLC 1.4. Member torsional loading (Mx) across the members is reduced between 6.93% and 9.36%, with the largest torsional load between all piles being reduced 9.36%. Overturning (Myz) loads across all members are very similar with and without flaps, with the difference between 0% and 0.68% with the largest overturning moment being reduced 0.68%. Axial loading ranged between a 1.29% increase to a 0.73% reduction with the largest load being reduced 0.5%. with flaps. Resolved shear loading (Fyz) was reduced 0.77% and 5.36% when using flaps, with the largest load reduced 0.76%. If all mudline members are to have the same design considerations, then flaps have shown an overall reduction in loads.

- The corner member loads are driven by DLC 1.4. Member torsional loading (Mx) across the members shows a range of responses, with an increase for the upwind member of 8.98% down to a decrease in the lateral member of 11.6% when using flaps. The largest load was reduced by 11.6%. Overturning (Myz) loads across all are reduced with with flaps, with the difference between 0.12% and 5.42% with the largest overturning moment being reduced 0.77%. Axial loading ranged between a 2.45% increase to a 0.66% reduction with the largest load being reduced 0.66%. with flaps. Resolved shear loading (Fyz) ranged between an increase of 1.18% and a decrease of 1.07% when using flaps, with the largest load reduced 0.74%. If all corner members are to have the same design considerations, then flaps have shown an overall reduction in loads.

Table 13: Stationary Hub Extreme Loads

		IPC		IFPC		Change from IPC
		Load Case	Load (kN/kNm)	Load Case	Load (kN/kNm)	
Mx	Max	dlc1.3eac1	46762	dlc1.3eac6	46878	0.25%
Mx	Min	dlc1.4ccb_1_d	-23325	dlc1.4ccb_2_a	-23609	1.22%
My	Max	dlc1.4bcc_2_b	1125390	dlc1.4bcc_2_b	1121000	-0.39%
My	Min	dlc1.4bcc_2_b	-1123150	dlc1.4bcc_2_b	-1119420	-0.33%
Mz	Max	dlc1.4bcc_2_b	148541	dlc1.4bcc_2_b	137207	-7.63%
Mz	Min	dlc1.4bcc_2_b	-167283	dlc1.4bcc_2_b	-160610	-3.99%
Myz	Max	dlc1.4bcc_2_b	1125700	dlc1.4bcc_2_b	1121370	-0.38%
Fx	Max	dlc1.4aac_2_b	9440.2	dlc1.4aac_2_b	9440.2	0.00%
Fx	Min	dlc1.4aac_2_d	-7418.9	dlc1.4aac_2_d	-7418.9	0.00%
Fy	Max	dlc1.4bcc_2_b	3222	dlc1.4ccb_2_d	3263.3	1.28%
Fy	Min	dlc1.4cbb_1_c	-1879.3	dlc1.3eac6	-1860.1	-1.02%
Fz	Max	dlc1.4bcc_2_b	-4410	dlc1.4bcc_2_b	-4409.5	-0.01%
Fz	Min	dlc1.4bcc_2_b	-11459	dlc1.4bcc_2_b	-11445	-0.12%
Fyz	Max	dlc1.4bcc_2_b	11861	dlc1.4bcc_2_b	11832	-0.24%

Table 14: Tower Base (Member 270) Extreme Loads

		IPC		IFPC		Change from IPC
		Load Case	Load (kN/kNm)	Load Case	Load (kN/kNm)	
Mx	Max	dlc1.4bcc_2_b	144163	dlc1.4bcc_2_b	133995	-7.05%
Mx	Min	dlc1.4bcc_2_b	-175466	dlc1.4bcc_2_b	-167803	-4.37%
My	Max	dlc1.4cca_1_c	518064	dlc1.4cca_1_c	515032	-0.59%
My	Min	dlc1.4ccc_2_c	-458308	dlc1.4ccc_2_c	-470216	2.60%
Mz	Max	dlc1.4aac_2_a	1329760	dlc1.4aac_2_a	1329760	0.00%
Mz	Min	dlc1.4bbc_2_d	-2057920	dlc1.4aac_2_d	-2027540	-1.48%
Myz	Max	dlc1.4bbc_2_d	2066740	dlc1.4bbc_2_d	2035420	-1.52%
Fx	Max	dlc2.2eb9	-33558	dlc2.2ea7	-33571	0.04%
Fx	Min	dlc1.4bcc_2_b	-45869	dlc1.4bcc_2_b	-45749	-0.26%
Fy	Max	dlc1.4bcc_2_b	18864	dlc1.4bcc_2_b	18696	-0.89%
Fy	Min	dlc1.4bcc_2_b	-21330	dlc1.4bcc_2_b	-21216	-0.53%
Fz	Max	dlc1.4bcc_2_b	4427.9	dlc1.4bcc_2_b	4855.5	9.66%
Fz	Min	dlc1.4cca_1_c	-3819.6	dlc1.4cca_1_c	-3797	-0.59%
Fyz	Max	dlc1.4bcc_2_b	21492	dlc1.4bcc_2_b	21383	-0.51%

Table 15: Blade Root Extreme Loads

		IPC		IFPC		Change from IPC
		Load Case	Load (kN/kNm)	Load Case	Load (kN/kNm)	
Mx	Max	dlc1.4bcc_2_b	163522	dlc1.4ccb_2_d	164514	0.61%
Mx	Min	dlc1.4bcc_2_b	-146154	dlc1.4bcc_2_b	-146334	0.12%
My	Max	dlc1.4bcc_2_b	740321	dlc1.4bcc_2_b	726441	-1.87%
My	Min	dlc1.4bcc_2_b	-750094	dlc1.4bcc_2_b	-727191	-3.05%
Mxy	Max	dlc1.4bcc_2_b	753377	dlc1.4bcc_2_b	742503	-1.44%
Fx	Max	dlc1.4bcc_2_b	10761	dlc1.4bcc_2_b	10516	-2.28%
Fx	Min	dlc1.4bcc_2_b	-10857	dlc1.4bcc_2_b	-10464	-3.62%
Fy	Max	dlc1.4bcc_2_b	2645.6	dlc1.4bcc_2_b	2598.6	-1.78%
Fy	Min	dlc1.4bcc_2_b	-3009.8	dlc1.4ccb_2_d	-3039.6	0.99%
Fxy	Max	dlc1.4bcc_2_b	10948	dlc1.4bcc_2_b	10790	-1.44%
Fz	Max	dlc1.4bac_2_d	9826.8	dlc1.4bac_2_d	9841.5	0.15%
Fz	Min	dlc1.4bcc_2_b	-2301.3	dlc1.4bcc_2_b	-2295	-0.27%

Table 16: Member 13 (Mudline Lateral) Extreme Loads

		IPC		IFPC		Change from IPC
		Load Case	Load (kN/kNm)	Load Case	Load (kN/kNm)	
Mx	Max	dlc1.4bcc_2_b	3188.3	dlc1.4bcc_2_b	2828.7	-11.3%
Mx	Min	dlc1.4bcc_2_b	-3888	dlc1.4bcc_2_b	-3576.1	-8.02%
My	Max	dlc1.4bcc_2_b	10918	dlc1.4bcc_2_b	11195	2.54%
My	Min	dlc1.4cca_1_c	2601.3	dlc1.4cca_1_c	2627.9	1.02%
Mz	Max	dlc1.4bcc_2_b	8580.6	dlc1.4bcc_2_b	8346.2	-2.73%
Mz	Min	dlc1.4bcc_2_b	-8173	dlc1.4bcc_2_b	-7939.9	-2.85%
Myz	Max	dlc1.4bcc_2_b	12188	dlc1.4bcc_2_b	12180	-0.07%
Fx	Max	dlc1.4cca_1_c	-2673.9	dlc1.4cca_1_c	-2765.2	3.41%
Fx	Min	dlc1.4bcc_2_b	-33125	dlc1.4bcc_2_b	-33553	1.29%
Fy	Max	dlc1.4bcc_2_b	4951.5	dlc1.4bcc_2_b	4737.2	-4.33%
Fy	Min	dlc1.4bcc_2_b	-4389.1	dlc1.4bcc_2_b	-3979.9	-9.32%
Fz	Max	dlc1.4bcc_2_b	5368.1	dlc1.4bcc_2_b	5037.2	-6.16%
Fz	Min	dlc1.4cbb_1_b	189.3	dlc1.4cca_1_c	258.4	36.50%
Fyz	Max	dlc1.4bcc_2_b	5541.9	dlc1.4bcc_2_b	5244.9	-5.36%

Table 17: Member 79 (Mudline Upwind) Extreme Loads

		IPC		IFPC		Change from IPC
		Load Case	Load (kN/kNm)	Load Case	Load (kN/kNm)	
Mx	Max	dlc1.4bcc_2_b	2770.4	dlc1.4bcc_2_b	2578.5	-6.93%
Mx	Min	dlc1.4bca_1_a	-2524.2	dlc1.4ccb_2_a	-2563.1	1.54%
My	Max	dlc1.4bcc_2_b	3287.6	dlc1.4bcc_2_b	3299.9	0.37%
My	Min	dlc1.4bba_1_b	-1861.5	dlc1.4bbb_1_a	-1719.9	-7.61%
Mz	Max	dlc2.2cb2	4429.9	dlc2.2cb1	4929.6	11.28%
Mz	Min	dlc1.4bbc_2_d	-23444	dlc1.4aac_2_d	-23324	-0.51%
Myz	Max	dlc1.4bbc_2_d	23497	dlc1.4aac_2_d	23337	-0.68%
Fx	Max	dlc1.4bcc_2_b	28048	dlc1.4bcc_2_b	27656	-1.40%
Fx	Min	dlc1.4bbc_2_d	-75223	dlc1.4aac_2_d	-74844	-0.50%
Fy	Max	dlc1.4bcc_2_b	12734	dlc1.4bcc_2_b	12602	-1.04%
Fy	Min	dlc1.4bcc_2_b	-8480.4	dlc1.4bcc_2_b	-8347.1	-1.57%
Fz	Max	dlc1.4bcc_2_b	2134.9	dlc1.4bcc_2_b	2032.5	-4.80%
Fz	Min	dlc1.4bcc_2_b	-2756.9	dlc1.4bcc_2_b	-2802.1	1.64%
Fyz	Max	dlc1.4bcc_2_b	12744	dlc1.4bcc_2_b	12619	-0.98%

Table 18: Member 112 (Mudline Downwind) Extreme Loads

		IPC		IFPC		Change from IPC
		Load Case	Load (kN/kNm)	Load Case	Load (kN/kNm)	
Mx	Max	dlc1.4ccb_1_d	2443.1	dlc1.4ccb_1_d	2448.1	0.20%
Mx	Min	dlc1.4bcc_2_b	-2856.7	dlc1.4bcc_2_b	-2639.5	-7.60%
My	Max	dlc1.3eab5	1623.6	dlc1.3eac5	1598.9	-1.52%
My	Min	dlc1.4bcc_2_b	-3709	dlc1.4bcc_2_b	-3507.3	-5.44%
Mz	Max	dlc1.4bbc_2_d	9726	dlc1.4aac_2_d	9628	-1.01%
Mz	Min	dlc1.4aac_2_b	-17962	dlc1.4aac_2_b	-17962	0.00%
Myz	Max	dlc1.4aac_2_b	17963	dlc1.4aac_2_b	17963	0.00%
Fx	Max	dlc1.4bbc_2_d	39845	dlc1.4aac_2_d	39596	-0.62%
Fx	Min	dlc1.4bcc_2_b	-64413	dlc1.4bcc_2_b	-63940	-0.73%
Fy	Max	dlc1.4bcc_2_b	13326	dlc1.4bcc_2_b	13228	-0.74%
Fy	Min	dlc1.4bcc_2_b	-8126.2	dlc1.4bcc_2_b	-7951.2	-2.15%
Fz	Max	dlc1.4bcc_2_b	2960.2	dlc1.4bcc_2_b	2779.9	-6.09%
Fz	Min	dlc1.4bcc_2_b	-2360.5	dlc1.4bcc_2_b	-2231.8	-5.45%
Fyz	Max	dlc1.4bcc_2_b	13358	dlc1.4bcc_2_b	13256	-0.76%

Table 19: Member 204 (Mudline Lateral) Extreme Loads

		IPC		IFPC		Change from IPC
		Load Case	Load (kN/kNm)	Load Case	Load (kN/kNm)	
Mx	Max	dlc1.4bcc_2_b	4085.1	dlc1.4bcc_2_b	3721.2	-8.91%
Mx	Min	dlc1.4bcc_2_b	-4375.7	dlc1.4bcc_2_b	-3966.2	-9.36%
My	Max	dlc1.4cca_1_c	11156	dlc1.4cca_1_c	11140	-0.14%
My	Min	dlc1.4bcc_2_b	2550	dlc1.4bcc_2_b	2450.5	-3.90%
Mz	Max	dlc1.4bcc_2_b	8369.1	dlc1.4bcc_2_b	8526.6	1.88%
Mz	Min	dlc1.4bcc_2_b	-8402.6	dlc1.4bcc_2_b	-8182.6	-2.62%
Myz	Max	dlc1.4cca_1_c	11275	dlc1.4cca_1_c	11261	-0.12%
Fx	Max	dlc1.4bcc_2_b	-2241.3	dlc1.4bcc_2_b	-1476.9	-34.1%
Fx	Min	dlc1.4cca_1_c	-32704	dlc1.4cca_1_c	-32614	-0.28%
Fy	Max	dlc1.4bcc_2_b	4201.2	dlc1.4ccb_2_d	4059.6	-3.37%
Fy	Min	dlc1.4bcc_2_b	-4025.6	dlc1.4bcc_2_b	-3997.7	-0.69%
Fz	Max	dlc1.4cbb_1_b	4471.2	dlc1.4cca_1_c	4385.5	-1.92%
Fz	Min	dlc1.4bcc_2_b	-600.6	dlc1.4bcc_2_b	-377.5	-37.2%
Fyz	Max	dlc1.4bcc_2_b	5116.5	dlc1.4bcc_2_b	5077.2	-0.77%

Table 20: Member 23 (Lateral Corner) Extreme Loads

		IPC		IFPC		Change from IPC
		Load Case	Load (kN/kNm)	Load Case	Load (kN/kNm)	
Mx	Max	dlc1.4bcc_2_b	1644.6	dlc1.4bcc_2_b	1557.2	-5.31%
Mx	Min	dlc1.4bcc_2_b	-2021.9	dlc1.4bcc_2_b	-1787.4	-11.60%
My	Max	dlc1.4cbb_1_b	10799	dlc1.4cca_1_c	10601	-1.83%
My	Min	dlc1.4bcc_2_b	298.2	dlc1.4bcc_2_b	810	171.63%
Mz	Max	dlc1.4bcc_2_b	6087.9	dlc1.4bcc_2_b	5869.7	-3.58%
Mz	Min	dlc1.4bcc_2_b	-8019.2	dlc1.4bcc_2_b	-8164.4	1.81%
Myz	Max	dlc1.4bba_1_a	11398	dlc1.4bba_1_a	11384	-0.12%
Fx	Max	dlc1.4bcc_2_b	-1167.5	dlc1.4bcc_2_b	-413.6	-64.57%
Fx	Min	dlc1.4cca_1_c	-34942	dlc1.4cca_1_c	-34841	-0.29%
Fy	Max	dlc1.4bba_1_c	457.2	dlc1.4bcc_2_b	462.1	1.07%
Fy	Min	dlc1.4baa_1_b	-349	dlc1.4baa_1_c	-333.2	-4.53%
Fz	Max	dlc1.4bcc_2_b	-239.5	dlc1.4bcc_2_b	-212.9	-11.11%
Fz	Min	dlc1.4cbb_1_c	-945.4	dlc1.4cca_1_c	-941.2	-0.44%
Fyz	Max	dlc1.4bba_1_b	964.5	dlc1.4cbb_1_c	954.2	-1.07%

Table 21: Member 215 (Downwind Corner) Extreme Loads

		IPC		IFPC		Change from IPC
		Load Case	Load (kN/kNm)	Load Case	Load (kN/kNm)	
Mx	Max	dlc1.4aaa_2_b	1080.5	dlc1.4aaa_2_b	1073	-0.69%
Mx	Min	dlc1.4aac_1_c	-991.3	dlc1.4aac_1_c	-989.9	-0.14%
My	Max	dlc1.4bcc_2_b	29294	dlc1.4bcc_2_b	29069	-0.77%
My	Min	dlc1.4bcc_2_b	-15193	dlc1.4bcc_2_b	-14894	-1.97%
Mz	Max	dlc1.4bcc_2_b	5700.2	dlc1.4bcc_2_b	5327.1	-6.55%
Mz	Min	dlc1.4bcc_2_b	-5684.2	dlc1.4bcc_2_b	-5259.6	-7.47%
Myz	Max	dlc1.4bcc_2_b	29350	dlc1.4bcc_2_b	29125	-0.77%
Fx	Max	dlc1.4bbc_2_d	46808	dlc1.4aac_2_d	46334	-1.01%
Fx	Min	dlc1.4bcc_2_b	-65483	dlc1.4bcc_2_b	-65259	-0.34%
Fy	Max	dlc1.4aca_1_d	220.3	dlc1.4ccb_1_c	210.3	-4.54%
Fy	Min	dlc1.4bcc_2_b	-325.6	dlc1.4bcc_2_b	-298.4	-8.35%
Fz	Max	dlc1.4bcc_2_b	897.8	dlc1.4bcc_2_b	893.3	-0.50%
Fz	Min	dlc1.4bcc_2_b	-2053.3	dlc1.4bcc_2_b	-2037.2	-0.78%
Fyz	Max	dlc1.4bcc_2_b	2057	dlc1.4bcc_2_b	2041.8	-0.74%

Table 22: Member 227 (Lateral Corner) Extreme Loads

		IPC		IFPC		Change from IPC
		Load Case	Load (kN/kNm)	Load Case	Load (kN/kNm)	
Mx	Max	dlc1.4bcc_2_b	1768.1	dlc1.4bcc_2_b	1597.5	-9.65%
Mx	Min	dlc1.4bcc_2_b	-1602.2	dlc1.4bcc_2_b	-1606.2	0.25%
My	Max	dlc1.4bcc_2_b	12785	dlc1.4bcc_2_b	12064	-5.64%
My	Min	dlc1.4cbb_1_b	1984.7	dlc1.4cca_1_c	2156.2	8.64%
Mz	Max	dlc1.4bcc_2_b	6610.2	dlc1.4bcc_2_b	6293.9	-4.79%
Mz	Min	dlc1.4bbc_2_d	-8446.4	dlc1.4bcc_2_a	-8521	0.88%
Myz	Max	dlc1.4bcc_2_b	13574	dlc1.4bcc_2_b	12838	-5.42%
Fx	Max	dlc1.4cca_1_c	-1222.1	dlc1.4cca_1_c	-1325.7	8.48%
Fx	Min	dlc1.4bcc_2_b	-34475	dlc1.4bcc_2_b	-35318	2.45%
Fy	Max	dlc1.4aac_2_b	355	dlc1.4aac_2_b	355	0.00%
Fy	Min	dlc1.4bbc_2_d	-653.7	dlc1.4bbc_2_d	-650.5	-0.49%
Fz	Max	dlc1.4cca_1_c	-293.7	dlc1.4cca_1_c	-295.8	0.72%
Fz	Min	dlc1.4bcc_2_b	-1014.1	dlc1.4bcc_2_b	-1020.9	0.67%
Fyz	Max	dlc1.4bbc_2_d	1024.7	dlc1.4ccc_2_b	1036.8	1.18%

Table 23: Member 229 (Upwind Corner) Extreme Loads

		IPC		IFPC		Change from IPC
		Load Case	Load (kN/kNm)	Load Case	Load (kN/kNm)	
Mx	Max	dlc1.4bcc_2_b	1018.2	dlc1.4ccb_1_d	972.7	-4.47%
Mx	Min	dlc1.4cba_2_b	-1049.2	dlc1.4ccb_2_c	-1143.4	8.98%
My	Max	dlc1.4bcc_2_b	27922	dlc1.4bcc_2_b	27727	-0.70%
My	Min	dlc1.4bcc_2_b	-15952	dlc1.4bcc_2_b	-15632	-2.01%
Mz	Max	dlc1.4bcc_2_b	4839.8	dlc1.4bcc_2_b	4485.7	-7.32%
Mz	Min	dlc1.4bcc_2_b	-5320.2	dlc1.4bcc_2_b	-5689.9	6.95%
Myz	Max	dlc1.4bcc_2_b	27929	dlc1.4bcc_2_b	27729	-0.72%
Fx	Max	dlc1.4bcc_2_b	28160	dlc1.4bcc_2_b	27894	-0.94%
Fx	Min	dlc1.4bbc_2_d	-83067	dlc1.4aac_2_d	-82522	-0.66%
Fy	Max	dlc1.4bcc_2_b	276.7	dlc1.4bcc_2_b	250	-9.65%
Fy	Min	dlc1.4bca_2_b	-181.1	dlc1.3eac4	-201.9	11.49%
Fz	Max	dlc1.4bcc_2_b	860.3	dlc1.4bcc_2_b	848.5	-1.37%
Fz	Min	dlc1.4bcc_2_b	-2048.5	dlc1.4bcc_2_b	-2050.6	0.10%
Fyz	Max	dlc1.4bcc_2_b	2048.7	dlc1.4bcc_2_b	2050.6	0.09%

DLC 1.4 (Extreme coherent gust with direction change) is a key driving load case for the 20 MW RWT in the analysis undertaken. However, as has been presented in [**8**], this load case likely does not make sense for large turbines and novel stochastic analysis of turbulent gusts is a more appropriate way of determining design loads. In fact, an examination of the six load cases leading to the largest blade flap loads (Figure 26) shows how much this load case can skew extreme loading relative to other load cases.

DLC 1.3 drives the asymmetric loading across the rotor if DLC 1.4 is excluded. However, due to the IFPC controller being tuned to achieve similar load reduction to the IPC controller in normal operation, the extreme turbulence of DLC 1.3 results in poor performance of the IFPC (see Table 24), with an increase in tower torsional moments of 8.49%. In DLC 1.3, the supervisory controller is disabled to ensure the turbine does not shutdown, so the load reduction features designed are not exercised. For this scenario, techniques as discussed in Section 5 should be pursued.

If DLC 1.3 is then removed from the analysis, indicative results can be seen in Table 25. During these extreme events, flap control has made significant contribution to asymmetric load reductions, with stationary hub Myz and tower base Mx load reducing 20% and 29% respectively.

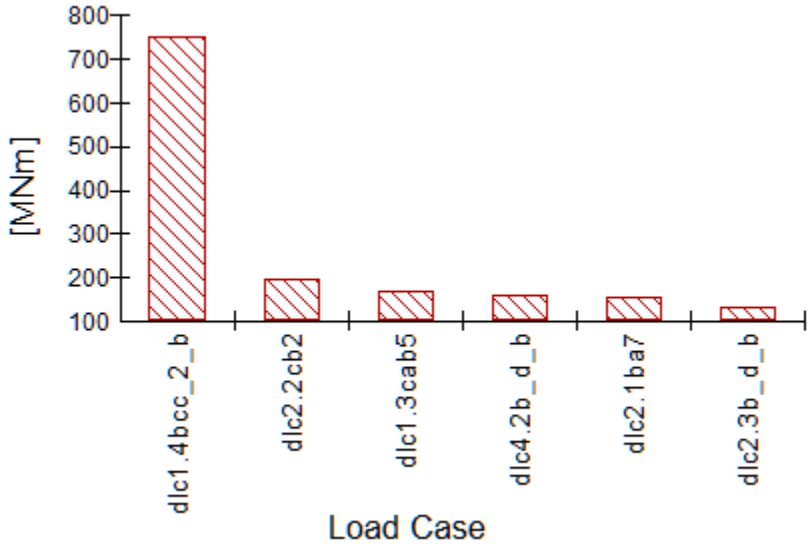

Figure 26: Blade Root My Extreme Load Histogram

Table 24: Extreme asymmetric loads not including DLC 1.4

	IPC		IFPC		% Change
	Case	Load (MNm)	Case	Load (MNm)	
Hub Myz	dlc1.3eaa1	119	dlc1.3eac6	117	-1.83%
Tower base Mx	dlc1.3eac2	115	dlc1.3eab6	125	8.49%

Table 25: Extreme asymmetric loads not including DLC 1.4 or DLC 1.3

	IPC		IFPC		% Change
	Case	Load (MNm)	Case	Load (MNm)	
Hub Myz	dlc2.2eb11	109	dlc2.2eb6	87	-19.55%
Tower base Mx	dlc2.2eb2	106	dlc2.1ec2	75	-28.65%

4.3 Conclusions

IFPC has been compared to IPC on the INNWIND 20 MW RWT on an advanced steel jacket in Bladed 4.8. The comparisons are made between lifetime weighted fatigue DELs and extreme loads, calculated using IEC design load guidelines. Loading results are taken on the stationary hub, blade root, tower base, jacket mudline members and jacket corner members.

The IFPC and IPC controllers are tuned to give similar results in fatigue load calculations and then IFPC is designed to reduce extreme loads during shutdowns that are caused by asymmetric rotor loading. In particular, hub tilting/yawing loads and tower member torsional loads. Design loads are driven by DLC 1.4. When DLC 1.4 is included in the DLC's analysed, hub yaw loading is reduced by 4%, tower base torsional loading is reduced by 4.37%, mudline member torsional loads are reduced 9.36% and corner member loads are reduced 11.6%.

If DLC 1.4 is excluded from the analysis, as it heavily skews the results and may not be valid for turbines of the 20 MW scale, DLC 1.3 dominates the asymmetric loads. The features designed for flap control are not exercised in this load case however, and so the benefits are not shown. In addition, the asymmetric loading can actually increase (for example the tower base torsional loading) when using IFPC if it is not designed to operate in extreme turbulence.

If DLC 1.3 Is also removed from the analysis, the performance of the IFPC controller becomes significantly stronger, reducing stationary hub Myz and tower base Mx loads by 20% and 29% respectively.

5.0 Evaluation of 20 MW LIR Wind Turbine with advanced control (NTUA)

In the present section, assessment of load reduction capabilities of an individual flap control feed-forward algorithm based on wind speed measurements obtained using a spinner anemometer, applied to the 20MW LIR turbine mounted on the Rambøll jacket, is performed.

The controller uses flap actuators with the aim to remove any deterministic source of load variation on blades, associated with the characteristics of the inflow. Such load variations are concentrated on multiples of the rotational frequency (p multiples) and they are mainly due to i) wind yaw misalignment - within the range that yaw control is not activated ii) ABL shear and iii) wind inclination. The aim of the controller is to assist operation of the conventional feedback individual pitch controller (IPC) and thereby reduce its control duty cycle. Then, IPC control is only employed for removing 1P excitation due to the rotational sampling of turbulence. Detailed description of the controller and its tuning procedure can be found in [**8**]. The only difference in the present implementation of the control loop with respect to the one presented in [**8**] is that 1P flap control is only performed while 2P flap control has been omitted. The controller originally tuned on the DTU 10MW RWT has been now re-tuned for the up-scaled 20MW LIR rotor.

Trailing edge (TE) flap control is performed on the outer part of the blade of the 20MW LIR. The blade of the LIR consists of new airfoil shapes, which have been specifically designed for the rotor under WP2. The relative thickness of the outer part of the blade is constant and equal to t/c=0.26. The camber line morphing shape presented in [**4**] is used. The flap extends to 30% of the section chord length. The spanwise extent of the flap is also 30% of the blade radius. The basic characteristics of the flap are detailed in Table 7. Flap motion is bounded in the range $[-10^0, +10^0]$. In addition, saturation limits have been imposed on the velocity of the flap motion to 20^0/s. In all configurations a delay of 0.1 s has been imposed on the flap motion in order to account for the dynamics of the flap actuator (through a first order filter in flap response).

Both fatigue and ultimate loads are considered in the analyses. Fatigue loads are assessed on the basis of IEC DLC 1.2 (normal operation with normal turbulence conditions NTM and normal sea state NSS) while ultimate loads are estimated through DLC 1.3 (normal operation with extreme turbulence conditions ETM and NSS) and DLC 1.6 (NTM combined with severe sea state SSS). For all wind speeds simulations for yaw angles 0^o, $+15^o$, and -15^o are performed. Simulated conditions and wind speeds are summarized in Table 8. It is noted that for all wind speeds and yaw angles two turbulent seeds are simulated. In Table 9, wave characteristics (in terms of significant wave height Hs and peak spectral period Tp) used in the simulations are provided for the different sea conditions and wind speeds.

For the IC 20MW LIR simulations are performed (a) for the baseline turbine without IPC and/or flap control (thereafter called “default”), (b) for the turbine with IPC only and (c) for the turbine with

combined IPC & spinner anemometer based flap control (thereafter called “spinner”). The aim of the analysis is i) to assess load reduction capabilities of the combined pitch/flap control loop against pure IPC and ii) to assess pitch actuator duty cycle reduction for IPC as a result of the operation of the flaps. Lifetime fatigue loads are calculated assuming the following Weibull parameters: C=11 m/s and k=2. Individual pitch or/and flap control is usually not recommended in the partial load region since the interaction of the pitch/flap controller with the basic power-speed controller could compromise power production. However, in order to assess load reduction capabilities at lower wind speeds in the present work pitch/flap operation has been also extended to wind speeds below rated.

Table 26: TE flap layout.

Flap configuration	
	20MW LIR
Chordwise extent	30%
Deflection angle limits	±10^{o}
Deflection speed limit	20^{o}/s
Spanwise length	42.5 m (~30% of blade length)
Spanwise location	90.0-132.5m (from rotor centre)
Airfoil	T260_0208

Table 27: Simulated DLCs.

DLC	Definition	Bins [m/s]	Yaw(deg)
1.2	NTM, NSS	7, 11, 15, 19, 23	0, +-15
1.3	ETM, NSS	11	0, +-15
1.6	NTM, SSS	11	0, +-15

Table 28: Definition of sea state.

NSS		
U [m/s]	Hs [m]	Tp [s]
5.0	1.14	5.78
7.0	1.25	5.67
9.0	1.40	5.71
11.0	1.59	5.81
13.0	1.81	5.98
15.0	2.05	6.22
17.0	2.33	6.54
19.0	2.62	6.85
21.0	2.93	7.20
23.0	3.26	7.60
SSS		
	9.40	13.70

Fatigue loads (Table 10-Table 12)

- Substantial reduction of the DEL of the flapwise bending moment is obtained both through IPC and combined IPC& spinner anemometer based flap control. For IPC&spinner flap control 26% reduction is obtained at 0^o yaw, 13.5% at $+15^o$ yaw and 35% at -15^o yaw. Overall higher reduction rates are noted as the wind speed increases. Slightly higher reduction rates are attained with pure IPC especially at higher wind speeds.
- A slight reduction of 1% is noted on the edgewise bending moment DEL with combined IPC&spinner flap control. Again, slightly higher reduction (3.3%) is attained with pure IPC.
- Blade torsion moment DEL significantly increases by spinner flap control at 0^o and -15^o yaw. A slight decrease is noted at $+15^o$ yaw. Maximum DEL increase rate of 82.6% is noted at -15^o yaw angle. Pure IPC has a decreasing effect on torsion moment. Maximum reduction of 13.5% is obtained at yaw -15^o.
- An increase in the tower fore-aft bending moment DEL is obtained both through IPC and combined IPC&spinner flap control. Both IPC and spinner flap control have been designed to reduce blade loads. Thus, no control logic exists in the design of the control loop that could effectively be used for the alleviation of the tower loads. The increase in the DEL of the fore-aft bending moment is 3.3%, 4.1% and 3% for pure IPC at 0^o, -15^o and $+15^o$ yaw respectively. For combined IPC&spinner flap the corresponding rates of increase are higher (5.9%, 7.0% and 3.2%). It is important to note that the recorded rates of tower fatigue load increase are higher

than those obtained for the 10MW RWT. In the latter case the increase of tower fatigue loads was found to be marginal.

- Generally higher side-side and yawing moments are obtained.
- Overall jacket base loads slightly increase. Interestingly, jacket first level X-braces X1 moments slightly decrease while axial X1 forces tend to increase.

Table 29: 20MW LIR turbine at yaw angle 0º. Lifetime DELs calculated for 20 years with Weibull parameters C=11 m/s and k=2, Wöhler coefficient m=4 for the tower and the jacket and m=10 for the blades and $n_{ref}=10^8$ cycles.

YAW= 0deg																				
		07.00m/s			11.00m/s			15.00m/s			19.00m/s			23.00m/s			Overall		
		default	ipc	spinner	default	ipc	spinner	default	ipc	spinner	default	ipc	spinner	default	ipc	spinner	default	ipc	spinner
ROOT BLADE	edge (kNm)	23466	-1.8%	-1.7%	25998	-3.7%	-3.0%	26111	-2.4%	-2.0%	26865	-1.5%	-1.1%	27909	-0.4%	-0.5%	25890	-1.9%	-1.6%
	flap (kNm)	10359	-25.5%	-24.1%	26300	-31.9%	-29.0%	30108	-33.4%	-28.0%	33691	-32.0%	-26.8%	37844	-29.0%	-25.3%	31238	-30.1%	-25.9%
	torsion (kNm)	303	-5.2%	3.7%	409	-13.8%	13.9%	460	-10.0%	24.8%	495	-7.4%	43.6%	550	-5.4%	60.9%	465	-7.5%	46.6%
BASE TOWER	side (kNm)	8670	-6.0%	-5.1%	6746	-3.6%	-4.1%	12534	6.1%	4.5%	19666	5.8%	4.4%	28199	5.8%	1.3%	16734	6.1%	3.4%
	fore (kNm)	27355	-0.9%	0.1%	58362	2.6%	4.2%	51998	3.7%	6.4%	55441	3.2%	6.6%	62822	3.3%	4.8%	50955	3.3%	5.9%
	yaw (kNm)	7673	-3.7%	-3.7%	15309	-1.3%	-0.3%	22016	-1.3%	2.5%	26755	0.0%	4.8%	31318	-0.3%	7.6%	22191	-0.5%	4.7%
JACKET BASE	Fz (kN)	1243	0.1%	1.4%	2382	0.6%	1.2%	2376	2.0%	4.9%	2734	2.4%	5.1%	3242	2.0%	2.7%	2380	2.3%	4.4%
	Mx (kNm)	173	-5.6%	-5.0%	335	-0.3%	0.7%	410	1.0%	3.8%	490	1.8%	5.4%	580	2.8%	8.3%	413	1.6%	5.3%
	Mz (kNm)	260	-2.3%	-1.4%	472	0.4%	1.3%	649	0.8%	2.9%	792	1.4%	2.3%	912	1.3%	1.7%	653	1.3%	2.3%
JACKET X1	Fz (kN)	114	-4.1%	-2.9%	238	1.0%	1.8%	326	3.6%	6.6%	394	4.1%	7.5%	468	2.2%	6.1%	329	3.4%	6.9%
	Mx (kNm)	3	-3.8%	-2.7%	6	-2.8%	-0.5%	6	-4.9%	-4.6%	7	-3.8%	-3.5%	9	-2.8%	-0.7%	6	-3.8%	-3.2%
	Mz (kNm)	6	-3.6%	-2.8%	10	-3.1%	-1.0%	15	-4.9%	-4.6%	19	-3.7%	-3.0%	24	-2.8%	-0.9%	16	-3.8%	-2.9%

Table 30: 20MW LIR turbine at yaw angle +15º. Lifetime DELs calculated for 20 years with Weibull parameters C=11 m/s and k=2, Wöhler coefficient m=4 for the tower and the jacket and m=10 for the blades and $n_{ref}=10^8$ cycles.

YAW= 15deg																				
		07.00m/s			11.00m/s			15.00m/s			19.00m/s			23.00m/s			Overall		
		default	ipc	spinner	default	ipc	spinner	default	ipc	spinner	default	ipc	spinner	default	ipc	spinner	default	ipc	spinner
ROOT BLADE	edge (kNm)	23268	-1.3%	-1.1%	25778	-2.9%	-2.7%	25898	-1.1%	-1.6%	26489	0.0%	-0.8%	27787	0.9%	-0.7%	25608	-0.7%	-1.2%
	flap (kNm)	9975	-22.2%	-22.5%	24416	-31.7%	-28.9%	28766	-22.5%	-19.5%	30220	-17.6%	-15.1%	31957	-10.2%	-8.1%	28279	-15.4%	-13.5%
	torsion (kNm)	303	-3.9%	1.5%	383	-11.0%	3.6%	429	-5.1%	-0.4%	449	-1.7%	-4.9%	500	0.2%	-12.2%	426	-2.4%	-3.9%
BASE TOWER	side (kNm)	8921	5.4%	5.4%	6877	2.4%	-0.6%	12302	3.2%	2.9%	18931	4.2%	3.5%	27160	3.0%	2.6%	16249	3.7%	3.3%
	fore (kNm)	26860	-2.8%	-0.4%	57697	1.9%	4.1%	59526	4.9%	5.8%	61099	2.6%	2.4%	69642	2.7%	2.5%	54702	3.0%	3.2%
	yaw (kNm)	7264	-2.7%	-3.8%	14339	-1.8%	-1.6%	21983	-0.4%	-0.7%	27107	0.9%	0.3%	31940	0.9%	-0.2%	22415	0.6%	0.0%
JACKET BASE	Fz (kN)	1225	-0.5%	0.8%	2366	2.3%	3.1%	2613	3.2%	4.0%	2908	1.8%	1.2%	3522	1.6%	1.2%	2512	2.1%	1.9%
	Mx (kNm)	169	-2.3%	-2.7%	307	-1.0%	-0.1%	400	1.6%	1.2%	480	2.5%	1.7%	587	1.9%	0.5%	405	1.9%	1.2%
	Mz (kNm)	259	0.0%	1.4%	457	0.5%	1.3%	654	0.9%	2.2%	787	0.9%	1.4%	934	0.9%	0.9%	656	0.8%	1.5%
JACKET X1	Fz (kN)	109	-3.5%	-3.1%	217	0.6%	1.5%	316	3.6%	2.7%	388	4.9%	3.5%	468	2.8%	1.1%	323	3.8%	2.4%
	Mx (kNm)	3	-7.1%	-6.2%	6	-5.3%	-3.0%	7	-3.2%	-0.8%	8	-4.0%	-3.4%	9	-2.6%	0.5%	7	-3.6%	-1.8%
	Mz (kNm)	6	-7.0%	-6.6%	9	-5.3%	-3.1%	15	-3.0%	-1.0%	19	-3.8%	-3.3%	24	-2.6%	0.3%	16	-3.5%	-1.9%

Table 31: 20MW LIR turbine at yaw angle -15°. Lifetime DELs calculated for 20 years with Weibull parameters C=11 m/s and k=2, Wöhler coefficient m=4 for the tower and the jacket and m=10 for the blades and $n_{ref}=10^8$ cycles.

YAW=-15deg																				
		07.00m/s			11.00m/s			15.00m/s			19.00m/s			23.00m/s			Overall		
		default	ipc	spinner	default	ipc	spinner	default	ipc	spinner	default	ipc	spinner	default	ipc	spinner	default	ipc	spinner
ROOT BLADE	edge (kNm)	23383	-2.5%	-2.2%	26554	-4.4%	-3.1%	26474	-4.2%	-2.7%	27229	-3.1%	-0.8%	28586	-2.1%	3.4%	26244	-3.3%	-1.2%
	flap (kNm)	9676	-24.2%	-22.9%	26275	-35.7%	-35.1%	32177	-41.6%	-35.7%	38123	-43.6%	-34.7%	45572	-44.7%	-36.0%	35852	-43.5%	-34.9%
	torsion (kNm)	307	-6.2%	5.1%	407	-15.5%	23.6%	506	-15.1%	48.2%	570	-13.7%	83.3%	641	-12.8%	92.6%	531	-13.5%	82.6%
BASE TOWER	side (kNm)	9111	4.1%	4.6%	7306	4.9%	0.2%	12388	5.1%	3.9%	18995	5.9%	9.3%	28735	10.5%	24.8%	16470	7.8%	16.5%
	fore (kNm)	25949	-2.3%	-3.0%	54147	5.2%	4.6%	51038	4.1%	9.5%	53448	4.9%	8.3%	61013	4.9%	5.9%	48751	4.1%	7.0%
	yaw (kNm)	7363	-4.6%	-4.6%	14708	-0.8%	0.3%	21512	0.3%	10.0%	26661	2.2%	19.1%	31195	1.7%	14.6%	22050	1.2%	15.8%
JACKET BASE	Fz (kN)	1180	-1.8%	-0.9%	2251	2.4%	1.7%	2292	2.3%	8.5%	2553	2.9%	8.2%	3080	3.4%	5.6%	2250	2.5%	6.8%
	Mx (kNm)	170	-3.5%	-3.2%	320	1.0%	2.0%	416	0.9%	8.8%	493	2.4%	15.1%	583	3.2%	12.5%	414	2.0%	13.0%
	Mz (kNm)	220	-1.0%	1.4%	383	0.5%	0.3%	461	0.9%	5.1%	557	2.5%	7.3%	670	1.6%	5.8%	470	1.8%	5.7%
JACKET X1	Fz (kN)	112	-3.1%	-2.1%	231	2.9%	4.1%	327	3.6%	11.5%	399	3.5%	14.3%	466	2.6%	10.8%	331	3.0%	12.8%
	Mx (kNm)	3	-11.9%	-6.9%	6	-2.9%	-3.3%	6	-2.1%	-0.6%	7	-2.1%	0.8%	8	-2.2%	5.7%	6	-2.4%	1.2%
	Mz (kNm)	6	-11.5%	-6.9%	9	-3.3%	-3.0%	15	-2.0%	-0.4%	19	-2.4%	0.5%	24	-2.4%	5.5%	16	-2.5%	1.0%

Ultimate loads (Table 13)

- Extreme flapwise bending moment decreases both with IPC and combined IPC & spinner based flap control. A slightly higher reduction of the maximum flapwise moment (maximum moment is the ultimate design moment in this case) is obtained through pure IPC (4.7% reduction through spinner flap against 6.9% reduction with pure IPC). It is noted that driving DLC for the flapwise bending moment is DLC 1.3.
- An about 3% reduction of the maximum (ultimate load) edgewise bending moment is obtained both with IPC and combined pitch/flap control.
- A significant torsion moment increase (both min and max) is obtained through spinner flap control. This is again due to the twisting moment induced by flap motion.
- Overall combined blade moment decreases. Slightly higher load reduction is obtained through combined IPC & spinner flap as compared to pure IPC (7.1% for combined IPC & spinner flap against 6.7% for pure IPC).
- Maximum tower base fore-aft moment slightly decreases. Higher rate of load reduction (3.6%) is obtained through IPC. The rate of reduction with the combined IPC & spinner flap control is 1.4%.
- Ultimate tower base side-side and yaw moments significantly decrease
- An overall reduction of the combined tower base moment of 1.4% is obtained through combined IPC & spinner flap control. In case of pure IPC the load reduction rate is 3.5%. It is seen that combined tower base moment is essentially driven by fore-aft component. The rates of combined tower moment reduction are almost the same with those of the tower fore-aft moment component.
- Reduced jacket X1 loads are attained both with IPC and combined IPC & spinner flap control
- Reduced or neutral jacket base loads are obtained through both control strategies.

Table 32: 20MW LIR turbine. Min-max loads – Min and Max loads of the fatigue DLC 1.2 are also included.

			DLC 1-2			DLC 1-3			DLC 1-6			Overall		
			default	ipc	spinner	default	ipc	spinner	default	ipc	spinner	default	ipc	spinner
ROOT BLADE	edge (kNm)	max	25703	-0.7%	2.9%	33512	-2.7%	-2.8%	27198	-1.6%	-0.4%	33512	-2.7%	-2.8%
		min	-22061	0.7%	3.3%	-24760	-7.7%	-4.8%	-18429	-3.9%	-2.4%	-24760	0.7%	3.3%
	flap (kNm)	max	56379	-8.2%	-6.6%	67349	-6.9%	-4.7%	60687	-5.1%	-3.4%	67349	-6.9%	-4.7%
		min	-38043	-51.9%	-45.7%	-23854	-135.6%	-125.9%	-2687	998.6%	941.2%	-38043	-51.9%	-45.7%
	torsion (kNm)	max	438	-26.2%	141.1%	584	-18.3%	32.9%	478	-18.9%	38.7%	584	-19.0%	141.1%
		min	-709	-3.5%	56.1%	-591	-13.2%	18.6%	-431	-15.8%	9.8%	-709	-3.5%	56.1%
	combined (kNm)	max	58597	-7.1%	-6.5%	68420	-6.7%	-7.1%	63138	-7.1%	-6.5%	68420	-6.7%	-7.1%
BASE TOWER	side (kNm)	max	71832	-25.4%	-12.4%	40694	-26.0%	-19.3%	31614	-16.9%	-13.0%	71832	-25.4%	-12.4%
		min	-26668	-2.1%	-3.6%	640	97.2%	87.2%	6961	488.3%	214.7%	-26668	-2.1%	-3.6%
	fore (kNm)	max	249051	-2.2%	-1.0%	299097	-3.6%	-1.4%	266176	-2.2%	-1.0%	299097	-3.6%	-1.4%
		min	-25367	45.4%	31.9%	-8592	-50.9%	-20.8%	65188	-22.4%	-19.3%	-25367	45.4%	31.9%
	yaw (kNm)	max	39032	-44.8%	-36.3%	33725	-45.7%	-42.6%	22091	-45.6%	-43.3%	39032	-44.8%	-36.3%
		min	-44064	-14.2%	-6.4%	-30963	6.2%	2.5%	-18090	18.5%	16.0%	-44064	-14.2%	-6.4%
	combined (kNm)	max	249620	-2.2%	-1.0%	299614	-3.5%	-1.4%	266641	-2.2%	-1.0%	299614	-3.5%	-1.4%
JACKET BASE	Fz (kN)	max	-3862	-11.3%	-14.0%	-5116	-4.0%	2.7%	-8167	-4.9%	-3.5%	-3862	-11.3%	-14.0%
		min	-15130	-1.3%	-1.1%	-17571	1.5%	2.1%	-16817	-1.3%	-0.4%	-17571	1.5%	2.1%
	Mx (kNm)	max	1536	-8.4%	-11.6%	1866	13.1%	8.5%	1703	20.2%	14.2%	1866	-8.4%	-11.6%
		min	148	-38.6%	-28.4%	381	-37.7%	-38.4%	646	-34.5%	-31.1%	148	-38.6%	-28.4%
	Mz (kNm)	max	1784	0.6%	3.2%	2098	2.8%	3.3%	2066	0.1%	1.1%	2098	0.1%	1.1%
		min	-351	14.2%	6.7%	129	3.9%	5.8%	427	-1.6%	2.2%	-351	-1.6%	2.2%
	Mcomb (kNm)	max	2213	-9.4%	-7.9%	2627	-2.7%	-2.0%	2575	0.3%	1.5%	2627	0.3%	1.5%
JACKET X1	Fz (kN)	max	263	-37.5%	-30.5%	97	-24.3%	-18.5%	-105	-14.9%	-17.9%	263	-18.7%	-21.5%
		min	-929	-9.5%	-8.4%	-932	-9.3%	-4.3%	-768	23.3%	30.0%	-932	-9.5%	-8.4%
	Mx (kNm)	max	34	-6.3%	-1.4%	40	-2.7%	-4.4%	37	-1.9%	-1.4%	40	-1.9%	-1.4%
		min	8	-19.6%	-49.9%	10	-8.4%	-6.1%	17	-3.0%	-7.5%	8	-19.6%	-49.9%
	Mz (kNm)	max	21	-7.7%	-7.2%	18	-5.2%	-1.9%	45	-2.7%	-2.6%	45	-4.9%	-1.9%
		min	-19	-5.6%	-3.1%	-13	-6.8%	-11.2%	-38	-0.7%	-1.8%	-38	-5.6%	-3.1%
	Mcomb (kNm)	max	34	-6.3%	-2.0%	40	-4.4%	-5.5%	56	-3.8%	-3.9%	56	-3.8%	-3.9%

In Figure 4 and Figure 5 the flap and pitch motion characteristics of the different control strategies are presented for the NTM conditions. When combined IPC&spinner based flap control is applied, the flap motion reaches the saturation limit of $+10^{o}$ only at wind speeds higher than 15m/s (see Figure 4). The SDV of the flap angle is quit lower than the limit angle of 10^{o} (goes up to 4.5^{o}) indicating that flap motion stays below the limit angles most of the time and occasionally hits the upper bound.

In Figure 5 the SDV of the pitch motion is shown for all control strategies. It is seen that the SDV of the pitch motion in the full load region increases by 30-90% when pure IPC is applied as compared to the "default" case (no load control). When spinner based flap control is combined with IPC the rate of increase of the pitch motion with respect to the "default" case is almost one third that of the pure IPC. So, a significant saving of the duty cycle of the pitch actuator is achieved when spinner anemometer based flap control is engaged.

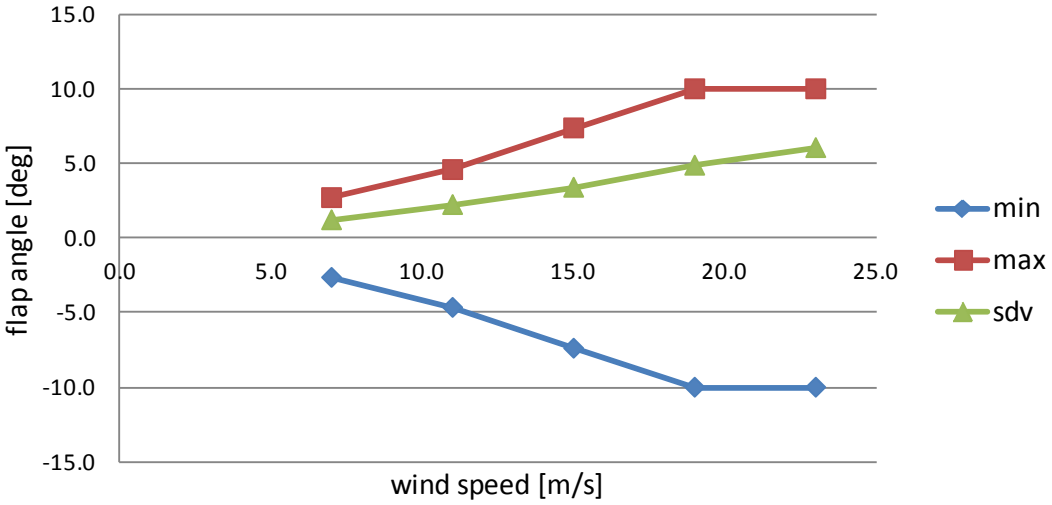

Figure 27: Flap angle variation.

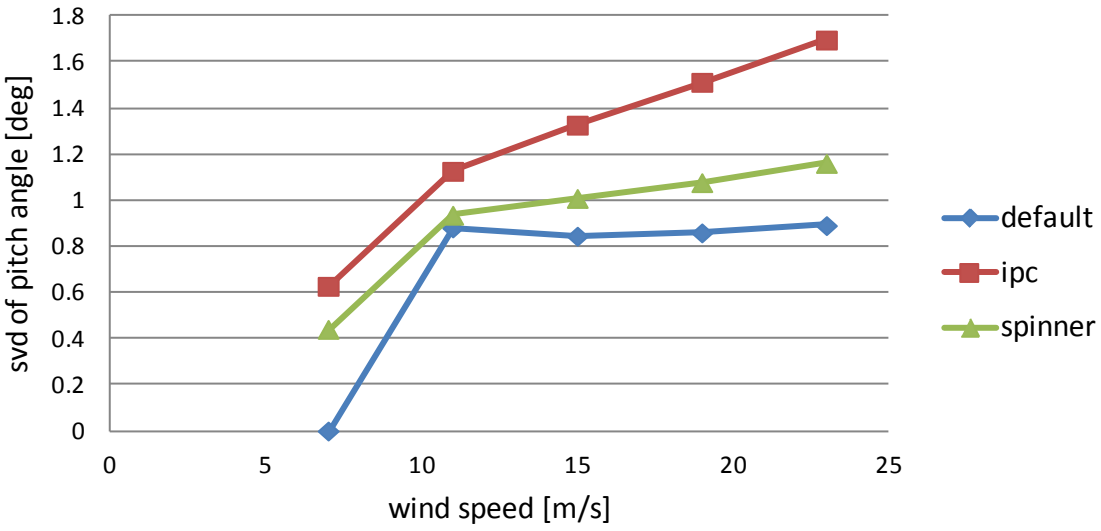

Figure 28: Pitch angle variation.

6.0 Evaluation of 20 MW Wind Turbine with Extreme Turbulence control (ECN)

Wind turbines are designed to withstand fatigue and ultimate loads resulting from a large variety of design conditions, called design load cases (DLC). These include both fatigue and ultimate loads experienced by the wind turbine components under different operational and environmental conditions that can occur during the lifetime of the wind turbine. The individual components of the wind turbine are designed to ensure that these design conditions will not lead to material failure. These design conditions include normal operation, but also operation under extreme conditions such as extreme wind gusts and direction changes as well as internal and external failures. Typically, wind turbine design engineers attempt to keep the fatigue and ultimate loads as low as possible in order to either

- ensure that all loads lie within the design loads envelope of existing turbine components, allowing them to use these and save costs with respect to using new tailor-made designs, or
- reduce on material costs in new designs

The wind turbine control system has a large effect on many of these DLCs [**17**]. For instance, during normal operation (DLC[1] 1.1-1.2) collective blade pitch control can be used to reduce the fatigue loads on the tower, individual pitch control can reduce the fatigue loading on the blades, and generator torque control can reduce fatigue loading on the drive train [**18**,**19**,**20**]. The control system can, however, also reduce the extreme loads in many critical DLCs such as those wherein

- extreme gusts are involved (DLC 1.4, 1.5): a gust detection algorithm, as the one proposed in [**21**,**22**], enables to react promptly to gusts by pitching the blades, avoiding rotor overspeeds and high loads.
- loss of electrical network (grid-loss) occurs during an extreme gust (In DLC 2.3): this results in a very demanding, often design-driving, situation with respect to the ultimate loads, e.g., on the tower. The (supervisory) controller could reduce these loads by shutting down the wind turbine using carefully designed pitch rate of the blades [**23**,**21**].
- failures in the blades are involved (DLC 2.2): this DLC leads to large asymmetric rotor loads, that have the potential of producing ultimate bending moments in the rotor shaft, on the main bearing, or at the yaw bearing. In this situation loads can be reduced by, (a) detecting the failure as fast as possible, and (b), design the stopping pitch trajectory to minimize the loading [**21**].

However, one of the most demanding design conditions is represented by DLC 1.3, where the turbine is simulated under extreme turbulence conditions. The turbulence intensity has a large effect on the loads, and is often a design driving load case for many components. For the 10MW Reference INNWIND.EU

[1] The DLC numbers are according to the definitions in IEC 61400-1 ed.3.

turbine [**24**], for instance, DLC 1.3 gives the ultimate loads at tower top and tower bottom (both fore-aft and side-to-side), blade root in flapwise direction, yaw bearing tilt and yaw, and produces the highest blade tip deflection [**24**]. To reduce loads on the tower, the use of a conventional tower fore-aft damping control loop has been proposed in the literature [**25**]. While this approach is more robust as it does not rely on algorithms for detecting the design condition, its overall effect on the ultimate loads remains limited. Moreover, the somewhat "relaxing" effect on the loads on the tower comes at the price of increased blade loading.

In [**26**] it is argued that a reduction of rated rotor speed is an effective way to reduce extreme loads under extreme turbulence, provided that an algorithm for detection of extreme turbulent wind is available. In this way, loads reduction is achieved at the expense of reduced power production in such conditions. The same line of reasoning is used in the present work. The proposed approach is based on a mechanism for detecting increased turbulence conditions, followed by reduction of the rated rotor speed. This is explained in Section 5.1. Subsequently, in Section 5.2 its performance is verified in two case studies, namely the 10MW and 20MW Reference INNWIND.EU [**24**,**27**] wind turbine models. Finally, Section 5.4 provides a discussion of the benefits from the developed control algorithm.

Remark. *It should be pointed out that according to the norm IEC61400-1 ed.3, the turbulence level in DLC 1.3 is to be increased until the loads become higher than those obtained from extreme loads extrapolation based on DLC 1.1. This method does not account for control algorithms that actively reduce loads during extreme turbulence conditions. The GL 2012 norm includes a load case with extreme turbulence model (DLC 1.2) but involves no extrapolation of extreme loads. This makes it possible to achieve load reduction using control algorithms as the one presented below. This control algorithm could also be very useful for use in turbines that are expected to operate during mild typhoons featuring higher turbulence levels.*

5.1 Extreme turbulence control

A new control strategy is proposed for reduction of extreme loads on wind turbine components during operation in extreme turbulence conditions, such as those specified in DLC 1.3 of the norm IEC 61400-1 ed.3. The control algorithm is based on estimation of the turbulence in the wind, followed by reduction of the rated rotor speed whenever this turbulence estimate exceeds certain limit. An optimization approach is developed to calculate the limit on the turbulence so as to achieve the best balance between alertness and false alarms, i.e. maximizing the loads reduction capabilities of the algorithm during extreme turbulence conditions and minimizing the chances for power losses during operation under normal turbulence.

The ETC concept is schematically represented in Figure 1, wherein the first three blocks are related to the estimation of the rotor-effective wind speed and turbulence. These are described in more detail in Section 5.1.1. The last block contains the mechanisms for detection of extreme turbulence conditions

and that for reduction of the rated rotor speed setpoint. These, together with the optimization method for determining the extreme turbulence detection limit, are discussed in Section 5.1.2.

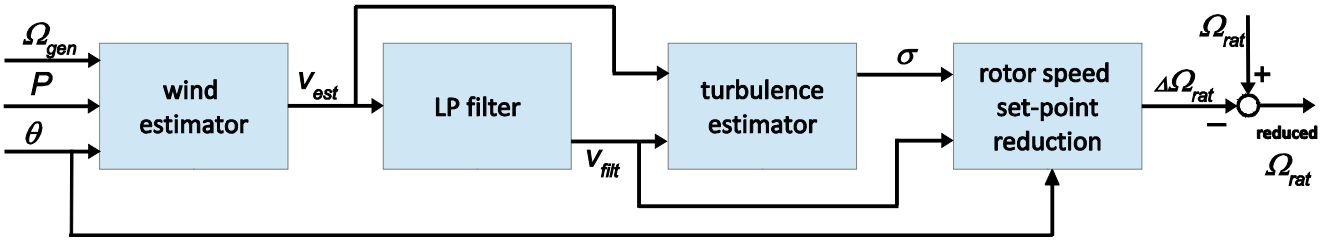

Figure 29 Schematic representation of the extreme turbulence control algorithm

5.1.1 Turbulence estimation

In order to obtain an estimate of the turbulence intensity (or, rather, the standard deviation of the wind speed), the *undisturbed* wind speed is required. This could be, for instance, obtained by using LiDAR measurements of the incoming wind inflow. However, as it may not be desirable to involve additional hardware due to costs, reliability aspects, or other arguments, the proposed algorithm is developed based only on the conventional measurements. More specifically, the undisturbed wind speed is first estimated (V_{est}) using the measurements of the generator speed (Ω_{gen}), blade pitch angle (θ) and electric power (P), as well as the aerodynamic power coefficient and a model of the energy losses. To this end, existing methods for estimation of the *rotor-effective* wind speed can be used, see e.g. [**28**,**29**].

Given the estimate of the wind speed V_{est}, an estimate of the turbulence is obtained in terms of an approximation of the variance of V_{est}, defined as:

$$\sigma^2 = \mathbb{E}\{(V_{est} - V_{mean})^2\}$$

Wherein $V_{mean} = \mathbb{E}\{V_{est}\}$ is the mean wind speed. To obtain an estimate of σ^2, first the mean wind speed is estimated by applying a low-pass filter to the rotor-effective wind speed estimate

$$V_{filt}(k) = F_V(q^{-1})V_{est}(k)$$

Here, k is the time sample, q^{-1} is the time-shift operator, and $F_V(q^{-1})$ is the applied low-pass filter. The estimate of the variance of the wind speed is then obtained as:

$$\hat{\sigma}^2(k) = F_\sigma(q^{-1})\big(V_{est}(k) - V_{mean}(k)\big)^2$$

where $F_\sigma(q^{-1})$ is a low-pass filter with a very low cutoff frequency (lower than that of F_V).

5.1.2 Extreme turbulence detection

To determine if the turbine operates under high turbulence, the variance estimate $\hat\sigma$ is compared to a wind-speed dependent thresholdσ_{lim}. The threshold will be allowed to depend on the average wind speed. i.e. $\sigma_{lim}^2\left(V_{filt}(k)\right)$, since the variance $\hat{\sigma}^2$ usually increases with the average wind speed. The norm IEC 61400-1 ed.3 specifies a linear dependency of the *standard deviation* of the wind speed $\hat{\sigma}^2$ on the average wind speed. Therefore, it seems appropriate to choose σ_{lim}^2 as a *quadratic* function of the average wind speed. However, for the considered interval of wind speeds (up to 25 m/s) the variance of the wind can also be approximated well enough by a linear function. Therefore, for the sake of design simplicity, a linear dependency of the threshold on the mean wind speed is suggested:

$$\sigma_{lim}^2\left(V_{filt}(k)\right) = a_\sigma V_{filt}(k) + b_\sigma, V_{filt}(k) \in \left[V_{on}, V_{off}\right],$$

where the design parameters a_σ and b_σ define the slope and offset of the threshold function σ_{lim}^2, and V_{on} and V_{off} define its domain of definition. In other words the ETC algorithm is only allowed to be active if the condition $V_{on} \leq V_{filt}(k) \leq V_{off}$ is met.

The condition for detection of extreme turbulence will, hence, be that the variance estimate $\hat{\sigma}$ is larger than the threshold σ_{lim}^2. However, it is not desirable to activate or deactivate ETC while the blades are being pitched at a high rate by the rotor speed control (e.g. in response to a sudden wind gust or wind dip). The reason for that is that by switching the ETC on or off will add additional pitch rate demand to that coming from the rotor speed control which, in combination with a wind gust or dip, can give rise to high loads. To avoid this, an additional condition on the pitch rate is added allowing/disallowing activation of the ETC algorithm. The following equation describes the conditions for activation and deactivation of the ECT algorithm as well as the corresponding rotor speed reduction $\Delta\Omega_{rat}^{unlim}$:

$$\Delta\Omega_{rat}^{unlim}(k) = \begin{cases} \Omega_{ETC}, & if\ \hat{\sigma}^2(k) \geq \sigma_{lim}^2(k)\ AND\ \left|\dfrac{\theta(k)-\theta(k-1)}{T_s}\right| \leq \dot{\theta}_{max} \\ 0, & if\ \hat{\sigma}^2(k) < \sigma_{lim}^2(k)\ AND\ \left|\dfrac{\theta(k)-\theta(k-1)}{T_s}\right| \leq \dot{\theta}_{max} \\ \Delta\Omega_{rat}^{unlim}(k-1), & otherwise \end{cases}$$

In the expression above, Ω_{ETC} is a chosen rotor speed reduction offset, i.e. the value by which the rated rotor speed Ω_{rat} will be reduced during extreme turbulence conditions (see Figure 29). The more the rated rotor speed is reduced, the lower the loads and the power production. In fact, one may let the rotor speed offset Ω_{ETC} depend on the mean wind speed, for instance to reduce the rotor speed at higher

winds more than at lower winds in situations where the loads are more prominent at higher winds, and vice versa.

To ensure that the changes in the rated rotor speed are carried out gradually, a rate limiter is applied as follows

$$\Delta\Omega_{rat}(k) = \Delta\Omega_{rat}(k-1) + T_s \max\left(-\dot{\Omega}_{rat}^{LB}, \min\left(\dot{\Omega}_{rat}^{UB}, \frac{\Delta\Omega_{rat}^{unlim}(k) - \Delta\Omega_{rat}(k-1)}{T_s}\right)\right)$$

wherein $\dot{\Omega}_{rat}^{LB} > 0$ and $\dot{\Omega}_{rat}^{UB}$ represent the lower and upper bound on the rate of change of the rated rotor speed, respectively.

Finally, it is pointed out that the parameters of the threshold σ_{lim}^2 need to be carefully selected to ensure optimal performance of the ETC algorithm. Choosing the threshold parameters too low results in increased alertness of the algorithm to turbulence variations and, therefore, lower loads in DLC 1.3. This is because the rated rotor speed reduction will occur earlier and will last longer than when the threshold is higher. However, the downside of too low a threshold is the higher probability of "false alarms", i.e. higher chance that the turbine will operate at decreased power production during normal operation in DLC 1.2. This is obviously undesirable as it would adversely affect the power curve. And the other way around: too high a threshold reduces the chance for missed power production in DLC 1.2, but also decreases the loads reduction capabilities in DLC 1.3. In order to allow for optimized balance between missed production and loads reduction, an optimization-based design procedure has been developed for the selection of the parameters a_σ and b_σ defining the threshold σ_{lim}^2. This is explained below.

5.1.3 Threshold optimization

The parameters a_σ and b_σ are determined by means of constrained optimization. The cost function that is minimized is the area below the line $\sigma_{lim}^2(V) = a_\sigma V + b_\sigma$ in a selected interval of wind speeds $[V_{LB}, V_{UB}]$, i.e.

$$J(a_\sigma, b_\sigma) = \int_{V_{LB}}^{V_{UB}} (a_\sigma V + b_\sigma)\, dV = 0.5 a_\sigma (V_{UB}^2 - V_{LB}^2) + b_\sigma (V_{UB} - V_{LB})$$

The constraint is that the relative time for which the detection condition $\hat{\sigma}^2(k) \geq \sigma_{lim}^2$ holds during normal operation (i.e. under normal turbulence conditions according to DLC 1.2) remains bounded by a desired limit $\Delta T_{false,max}$

$$\left|\{k: \hat{\sigma}^2(k) \geq a_\sigma V_{filt}(k) + b_\sigma\}\right| \leq \mathrm{K}_{total} \Delta T_{false,max}.$$

In the expression above K_{total} is the total number of samples in the data used for optimizing the ETC parameters, and the notation $|S|$ is used to denote the number of members of a set S. For instance, by selecting $\Delta T_{false,max}$=0.001 during normal operation the turbine will operate at reduced rated rotor speed at most 0.1% of the time, which implies a total power production loss of no more than 0.1% (power production loss will not be incurred for rotor speeds below the reduced rated speed ($\Omega_{rat} - \Delta\Omega_{rat}$). In other words, the optimization aims at maximizing the alertness of the ETC algorithm (minimizing the threshold) for an acceptable power production loss during normal operation. It should be pointed out that $\Delta T_{false,max}$ can also be selected zero, ensuring no power loss in DLC 1.2. This will, of course, in turn reduce the alertness of the ETC algorithm, limiting its performance during extreme turbulence conditions in DLC 1.3.

The following procedure can be used for the solving above-mentioned optimization problem and evaluate its performance. Notice that the filters F_σ and F_V should have been selected before this optimization process is started as they influence the outcome.

Step 1. Perform a complete DLC1.2 and DLC 1.3 calculation using the controller with ETC disabled, and record (at least) the following internal controller variables: estimated rotor-effective wind speed V_{est}, filtered wind speed V_{filt}, and the estimate of the turbulence variance $\hat{\sigma}^2$. The DLC 1.2 calculations will be used to optimize the ETC algorithm parameters, while the DLC 1.3 simulations will be used in Step 4 as reference for analyzing the load reduction capabilities of the ETC algorithm.

Step 2. Select a desired $\Delta T_{false,max}$ that limits the power production loss due to ETC in DLC1.2, and interval of wind speeds $[V_{LB}, V_{UB}]$ for which the ETC threshold parameters are to be optimized.

Step 3. Optimize the ETC threshold parameters (a_σ, b_σ) for the range of wind speeds $[V_{LB}, V_{UB}]$ by numerically solving the constraint optimization problem above.

Step 4. The performance of the ETC algorithm with optimized parameters (a_σ, b_σ) is verified using DLC 1.2 and DLC1.3 simulations with ETC enabled. The DLC 1.2 simulations are used to check if the power production loss during normal production is indeed limited by what is considered acceptable (relative time with production loss less than $\Delta T_{false,max}$). The simulations from DLC 1.3 are used to analyze the extreme loads and compare these to the loads in the reference case (without ETC), performed at Step 1, in order to evaluate the load reduction capabilities of the ETC algorithm.

One simple way to perform the constraint optimization in Step 3 is by optimizing one of these two parameters (a_σ, b_σ) at a time while keeping the other one constant, and iterate between them until

convergence. The optimization of a single parameter could be done using, for instance, a bisection algorithm. It offers a simple and effective way of approaching the underlying nonlinear programming problem. For one optimized parameter, the idea is to start with an initial search interval and iteratively halve the length of this interval. More specifically, suppose that a_σ is being optimized for a fixed $b_\sigma = b_\sigma^*$. Then an initial search interval could be chosen as $[a_\sigma^{LB}, a_\sigma^{UB}]$ wherein $a_\sigma^{LB} = 0$ and a_σ^{UB} is selected high enough to ensure that the constraint in the equation above holds. At the *i*-iteration the constraint is checked for $\left(a_\sigma^{(i)} = 0.5(a_\sigma^{LB} + a_\sigma^{UB}), b_\sigma = b_\sigma^*\right)$. If the constraint is not satisfied, the lower bound is increased $\left(a_\sigma^{LB} \leftarrow a_\sigma^{(i)}\right)$, and otherwise the upper bound is decreased $\left(a_\sigma^{UB} \leftarrow a_\sigma^{(i)}\right)$. The iterations continue until sufficient accuracy is reached (i.e. length of interval, $a_\sigma^{LB} - a_\sigma^{UB}$, gets small enough). The optimized value for parameter a_σ is then taken as the upper bound a_σ^{UB} (as the constraint is not satisfied at the lower bound a_σ^{LB}). Next, b_σ is optimized in the same way my keeping a_σ fixed, and so on.

A better understanding of the optimization process can be obtained in Section 5.3 in which the optimization is applied to two test cases.

5.2 Results

In this section the ETC algorithm is designed and its performance is analyzed on two case studies: with the INNWIND.EU 10MW reference wind turbine (RWT) model and the INNWIND.EU 20MW RWT model. Besides the difference in turbine size, the two test cases differ also in the turbulence classes (INNWIND.EU 10MW is class 1A, while the 20MW counterpart is class 1C). This allows getting a good understanding of the potential benefits from ECT. The main parameters of these turbine models are summarized in Table 33.

Table 33: Main parameters of INNWIND.EU 10MW and 20MW turbine models

Parameter	INNWIND.EU 10MW RWT	INNWIND.EU 20MW RWT
Rotor diameter	23.73	99.4
Rated power	10MW	20MW
Cutin rotor speed	6 rpm	4.2 rpm
Rated rotor speed	9.6 rpm	7.13 rpm
Wind turbine class	1A	1C

5.2.1 Test case INNWIND.EU 10MW reference turbine

In this test case the ETC algorithm is designed and tested using the INNWIND.EU 10MW RWT model.

ETC optimization for INNWIND.EU 10MW RWT

The optimization approach for ETC design, explained in Section 5.1.3, is applied to the INNWIND.EU 10MW RTW model using DLC 1.2 simulations with the Phatas software. Figure 30 and Figure 31 are provided to better understand this process. In both of these figures the thin lines represent the estimated turbulence variance $\hat{\sigma}^2$ plotted against the filtered wind speed V_{filt} for all DLC 1.2 load cases, i.e. one line per DLC1.2 simulation. The difference between the two figures is the value of the parameter $\Delta T_{false,max}$ used in the optimization: in Figure 30 the results are given for $\Delta T_{false,max} = 0$ (implying that no power loss is tolerated under normal operating conditions in DLC 1.2), while the results in Figure 31 (left) are obtained for $\Delta T_{false,max} = 0.005$ (meaning that a power loss of at most 0.5% is considered acceptable in DLC 1.2).

In both Figure 30 and Figure 31, the thick lines represent threshold function $\sigma_{lim}^2\left(V_{filt}(k)\right)$ for different value of the parameters a_σ and b_σ. More specifically, the dash cross-marked (blue) lines correspond to minimizing the offset parameter b_σ for fixed $a_\sigma = 0$, which is done to obtain an upper limit of the initial search interval for the parameter b_σ. Similarly, the dash circle-marked (red) lines give σ^2 wherein the slope parameter a_σ has been minimized with fixed $b_\sigma = 0$, which gives an upper limit for the initial search interval for a_σ. Finally, unmarked dashed line (black) depict the final threshold σ^2 with both parameters a_σ and b optimized. Observe that the final values for the optimized parameters are lower than the initial upper bounds.

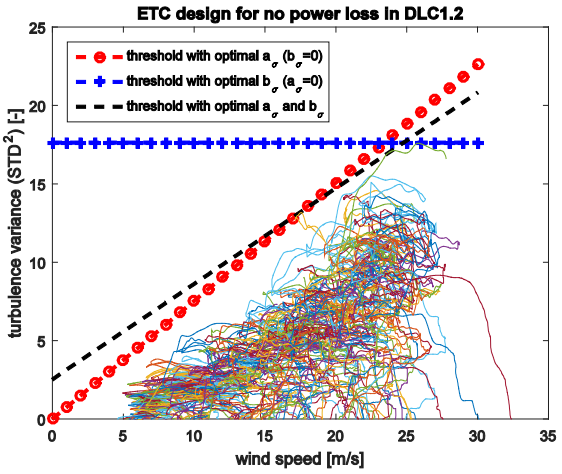

Figure 30 ETC threshold for INNWIND.EU 10MW RWT, conservative optimization: the threshold is selected to make sure that ETC will never trigger in DLC 1.2 (no missed production)

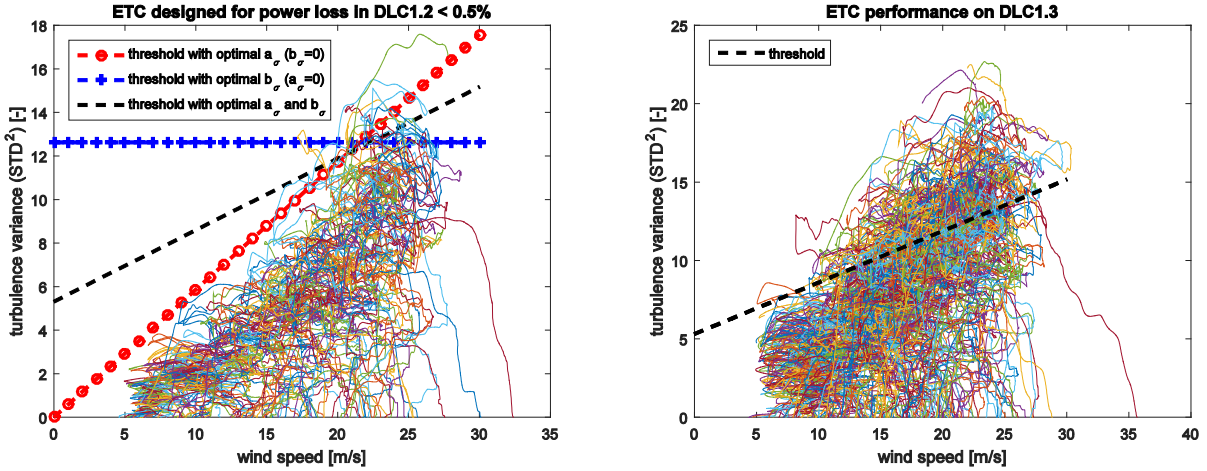

Figure 31 ETC threshold for INNWIND.EU 10MW RWT, balanced optimization: the threshold is selected lower, resulting in some small production loss (<0.5\%) in DLC 1.2 (left), but increased alertness in DLC 1.3 (right)

It can be observed from Figure 30 that the optimized threshold lies above the turbulence variance (thin lines) for all DLC 1.2 simulations, as expected for the selected zero power loss tolerance $\Delta T_{false,max} = 0$. In Figure 31 (left) on the other side, it is evident that the allowed power loss of 0.5% ($\Delta T_{false,max} = 0.005$) will take place at higher wind speeds above 15 m/s where the estimated wind turbulence lies occasionally above the threshold. The region of wind speeds at which the allowed power loss is incurred is controlled by the parameters V_{LB} and V_{UB}, which define the objective function in Section 5.2.3. For this test case the DLC 1.3 simulations with the 10MW INNWIND.EU model indicated a clear trend of the ultimate loads on tower and shaft increasing with the average wind speed, as discussed in more detail in the next section (see already the right-hand side plots in Figure 32. It was therefore considered in this case appropriate to sacrifice some small power production at high wind speeds, which have a lower probability of occurrence, in order to achieve a more pronounced reduction of ultimate loads. After some iterations with the tuning parameters, the ETC algorithm has finally been optimized for the wind speed region between 18 and 25, with acceptable power loss of 0.5% in DLC 1.2. These, and the remaining ETC parameters, are summarized in Table 34.

Parameter	Unit	Value
$F_V(q^{-1})$	-	$\frac{0.01q^{-2} - 0.02q^{-1} + 0.01}{q^{-2} - 1.9995q^{-1} + 0.9995}$
$F_\sigma(q^{-1})$	-	$\frac{5.10^{-5}}{q^{-1} + 0.9995}$
T_s	s	0.01
V_{LB}	m/s	18
V_{UB}	m/s	25
$\Delta T_{false,max}$	-	0.005
Ω_{ETC}	rpm	2
a_σ	m/s	0.3284
b_σ	m^2/s^2	5.3125

V_{on}	*m/s*	0
V_{off}	*m/s*	100
$\dot{\Omega}_{rat}^{LB}$	*rpm/s*	0.1
$\dot{\Omega}_{rat}^{UB}$	*rpm/s*	0.1
$\dot{\theta}_{max}$	*deg/s*	100

Table 34 ETC parameters for the INNWIND.EU 10MW RWT

The effectiveness of the optimized threshold function $\sigma_{lim}^2\left(V_{filt}(k)\right)$ during extreme turbulence conditions in DLC 1.3 will be evaluated by inspecting the ultimate loads in this loads case in the next section. At this point, however, one can already see from Figure 31 (right) that under DLC 1.3 the threshold is significantly lower with respect to the turbulence variances there (thin lines), implying that rotor speed derating will be in place during a large part of the DLC 1.3 simulations.

ETC performance analysis for INNWIND.EU 10MW RWT

To evaluate the performance of the ETC algorithm, simulations are performed with and without the ETC activated, as explained in Section 5.1.3. To this end, DLC1.2 and 1.3 have been simulated. The DLC1.2 simulations are used to verify that the ETC algorithm does not influence the performance of the wind turbine in a negative way during normal operation, besides the accepted loss of energy production defined by the parameter $\Delta T_{false,max}$ in the ETC optimization. A power production loss of no more than 0.5% is considered acceptable during DLC1.2, imposed by selecting $\Delta T_{false,max} = 0.005$ (see above). Increase of fatigue loads in DLC 1.2 is considered undesirable.

Table 35 summarizes the energy yield and fatigue loads on the main wind turbine components based on DLC 1.2 simulations, both in the reference case without ETC (column **REF**) and in the case with ETC activated (column **ETC**). The coordinate system used is the Germanischer Lloyd coordinate system. The last column (reduction) indicates the relative decrease of the corresponding indicator obtained under ETC as compared to the reference case. Clearly, the fatigue loads do not increase under ETC, and the power loss is less than 0.5%.

Component	**Unit**	**REF**	**ETC**	**ratio [%]**
DEQL blade flap	MNm	23.73	23.58	99.4
DEQL blade lead	MNm	20.13	20.09	99.77
DEQL blade XY	MNm	22.27	22.21	99.7
DEQL blade torsion	MNm	0.3697	0.3674	99.39
DEQL tower fore-aft	MNm	11.71	11.63	99.3
DEQL tower sideward	MNm	3.157	2.443	77.4
DEQL tower XY	MNm	5.668	5.558	98.06
DEQL shaft Y	MNm	14.1	14	99.34
DEQL shaft Z	MNm	14.2	14	99.16

DEQL shaft YZ	MNm	8.64	8.59	99.36
DEQL tower top tilt	MNm	11.4	11.3	99.34
DEQL tower top yaw	MNm	10.9	10.9	99.4
Energy capture 10-min	MWh	1.12	1.11	99.57

Table 35 Summary of energy yield and 600-cycles damage equivalent loads for INNWIND.EU 10MW RWT based on DLC 1.2

Next, the ultimate loads are evaluated based on DLC 1.3 simulations. The energy yield is not of importance here, only the extreme loads and deflections. Table 36 summarizes these for the selected main components. Clearly, very significant reductions of ultimate loads on tower and shaft are observed of well above the 20%.

Component	**Unit**	**REF**	**ETC**	**ratio [%]**
EXTR blade flap	MNm	66.3	66.8	100.8
EXTR blade lead	MNm	28.82	28.29	98.16
EXTR blade XY	MNm	67.82	68.32	100.7
EXTR blade torsion	MNm	0.7894	0.77	97.54
EXTR tower fore-aft	MNm	60.45	46.07	**76.21**
EXTR tower sideward	MNm	18.62	17.9	96.16
EXTR tower XY	MNm	60.5	46.44	**76.76**
EXTR shaft Y	MNm	49.9	41.7	**83.59**
EXTR shaft Z	MNm	58.4	44.8	**76.8**
EXTR shaft YZ	MNm	58.7	46.2	**78.74**
EXTR tower top tilt	MNm	60.9	46.5	**76.39**
EXTR tower top yaw	MNm	46	41.6	**90.38**
EXTR tip deflection	m	13.5	13	96.23

Table 36 Summary of ultimate loads for INNWIND.EU 10MW RWT based on DLC 1.3

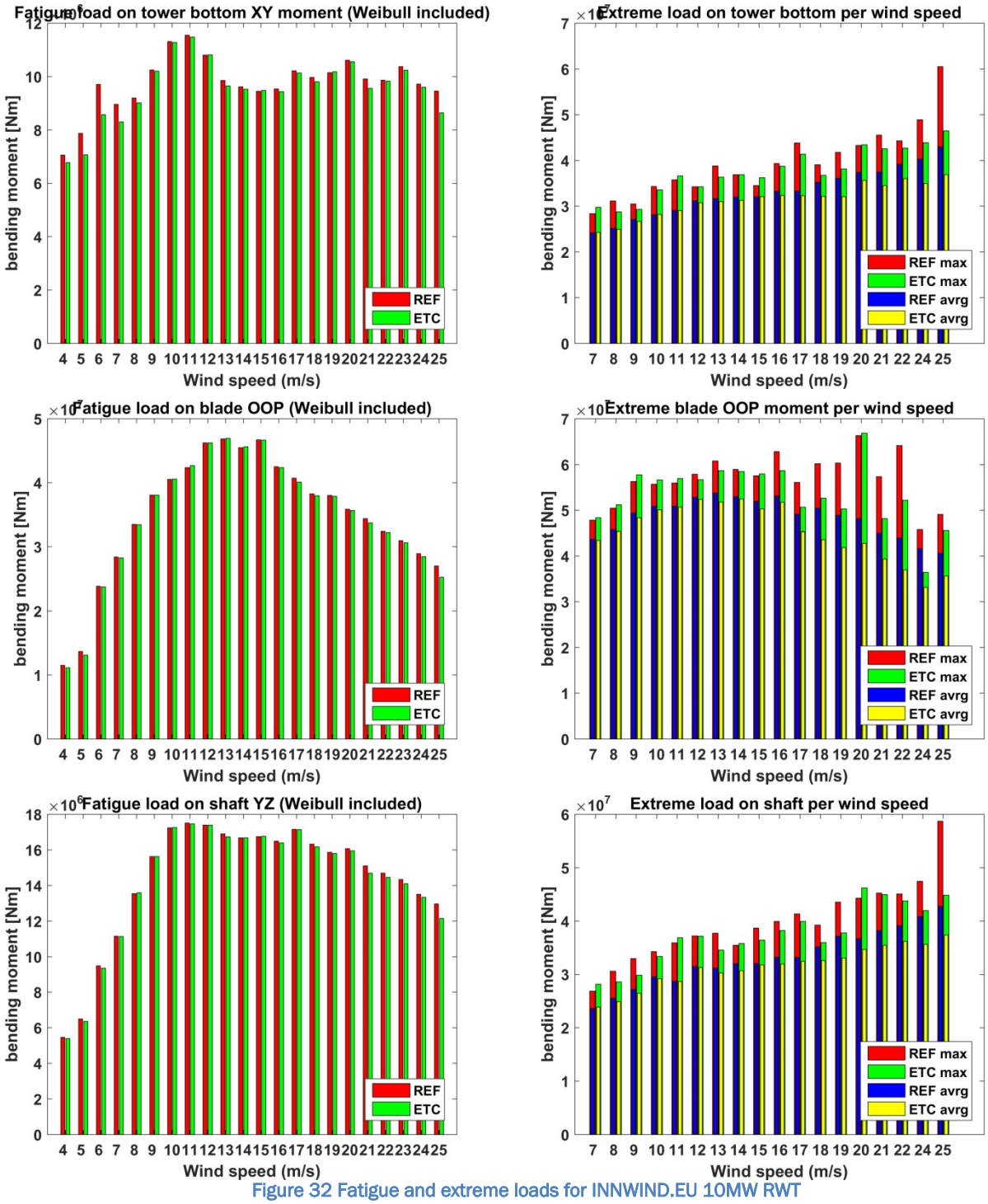

Figure 32 Fatigue and extreme loads for INNWIND.EU 10MW RWT

For more in-depth analysis of the results, Figure 32 is provided. The figure plots the fatigue loads (left hand side plots) and the ultimate loads (right-hand side plots). These are depicted as function of the average wind speed for the tower bottom XY moment (plots on top), blade root out-of-plane (OOP) moment (middle plots), and the shaft YZ moment (bottom plots). The bars in the plots represent the reference case without ETC (red bars) and the case with ETC active (green bars). For the ultimate loads in the right column, besides the loads' maxima over the different realizations (seeds) for a given wind speed (red and green bars) also the average values of the highest loads over the wind speed realizations are provided (blue and yellow bars) for more insight. It can be observed from the figure that the fatigue loads under ETC remain comparable to the reference case. For the ultimate loads, loads reduction is generally observed under ETC, primarily at wind speeds above 15 m/s for which the ETC algorithm is optimized. The load reduction trend is well visible by looking at the highest loads averaged over the wind realizations (compare blue to yellow bars) as the effect of occasional spikes in the loads are less prominent there. For the actual ultimate loads the results are somewhat less predictable (compare red to green bars): there is a very significant reduction of loads on the tower and shaft at cutout wind speeds, while at the same time no load reduction is achieved at the blades (see peak load at 20 m/s in the extreme blade OOP in Figure 24, which the ETC algorithm has failed to reduce).

5.2.2 Test case INNWIND.EU 20MW reference turbine

Next, the ETC algorithm is applied to the INNWIND.EU 20MW RWT model. Besides the larger size, this model has a wind turbine class 1C, featuring a lower turbulence intensity than the 10MW model (see Table 33). For the ETC algorithm, this is an important difference because the extreme turbulence in DLC 1.3 is now closer to the normal turbulence in DLC 1.2 in absolute sense, making it more difficult to differentiate between the two. The ETC design becomes more involved with respect to proper selection of the tuning parameters (V_{LB}, V_{UB} and $\Delta T_{false,max}$), and the benefit will in general be less pronounced.

ETC optimization for INNWIND.EU 20MW RWT

The optimization of the ETC threshold, explained in Section 5.1.3, has been applied to the INNWIND.EU 20MW RWT model. In selecting the tuning parameters in the optimization (V_{LB}, V_{UB} and $\Delta T_{false,max}$), similar considerations are used as for the INNWIND.EU 10MW RTW model above: small power loss in DLC 1.2 is considered acceptable, provided that the fatigue loads there do not increase and a significant reduction of ultimate loads is realized in DLC 1.3.

Contrary to the situation with the INNWIND 10MW RWT model, the ultimate loads on the tower no longer increase monotonically with the wind speed (see right-hand side plots in Figure 34, which will be discussed in more detail in the next section). In this case, the highest loads on tower and blades occur at just above rated wind speeds. If one aims to reduce ultimate loads on tower and blades using the ETC algorithm, one needs to optimize its performance in the region of wind speeds between 9 and 20 m/s. To reduce ultimate loads for these wind speeds, the threshold needs to be optimized for this region, which offers less flexibility than when optimizing it for higher winds speeds. The reason for

this is that the lower wind speed has a higher probability of occurrence, and hence reducing the threshold there will have a larger effect on the power loss in DLC 1.2 than when the threshold is reduced at higher wind speeds. After some iteration with the tuning parameters, the ETC algorithm has finally been optimized for the wind speed region between 9 and 11.5, with acceptable power loss of 0.4% in DLC 1.2. These, and the remaining ETC parameters, are summarized in Table 37.

Parameter	Unit	Value
$F_V(q^{-1})$	-	$\frac{0.01q^{-2} - 0.02q^{-1} + 0.01}{q^{-2} - 1.9995q^{-1} + 0.9995}$
$F_\sigma(q^{-1})$	-	$\frac{5.10^{-5}}{q^{-1} + 0.9995}$
T_s	*s*	0.01
V_{LB}	*m/s*	9
V_{UB}	*m/s*	11.5
$\Delta T_{false,max}$	-	0.004
Ω_{ETC}	*rpm*	1
a_σ	*m/s*	0.5646
b_σ	m^2/s^2	-2.4375
V_{on}	*m/s*	9
V_{off}	*m/s*	100
$\dot{\Omega}_{rat}^{LB}$	*rpm/s*	0.05
$\dot{\Omega}_{rat}^{UB}$	*rpm/s*	0.1
$\dot{\theta}_{max}$	*deg/s*	1

Table 37 ETC parameters for the INNWIND 20MW RWT

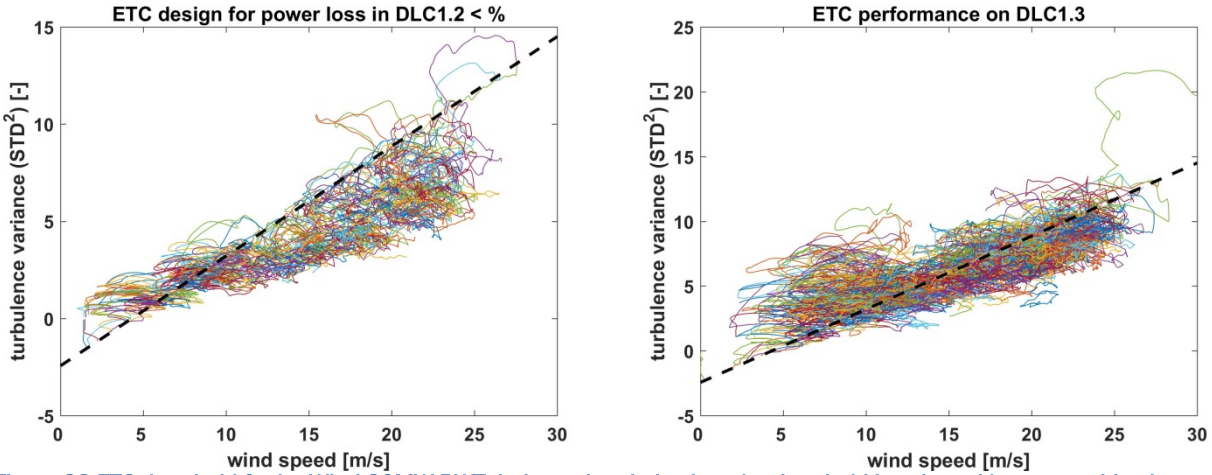

Figure 33 ETC threshold for InnWind 20MW RWT, balanced optimization: the threshold is selected lower, resulting in some small production loss (<0.5\%) in DLC 1.2 (left), but increased alertness in DLC 1.3 (right)

Figure 33 (left) provides a visualization of the optimized threshold function together with the estimated turbulence variations, obtained by carrying out DLC 1.2 simulations with the INNWIND 20MW RWT

using Phatas. The few lines lying well above the threshold at wind speeds above 20 m/s will not contribute noticeably to the power production loss in DLC 1.2 due to their low probability of occurrence. At lower winds (below rated), however, long periods of operation at reduced rated rotor speed are not desirable. To limit the power loss at below rated winds, the wind speed V_{on} for activation of ETC is set to 9 m/s (see Table 37). This will avoid rotor speed reduction below this wind speed.

Under extreme turbulence conditions (DLC 1.3), the estimated turbulence variance will be often higher than the threshold function and the turbine will operate at reduced rotor speed for long periods of time (see Figure 33 (right)). The actual effect of this on the ultimate loads in DLC 1.3 is discussed in the next section.

ETC performance analysis for INNWIND 20MW RWT

In this section, the performance of the ETC algorithm is evaluated. To this end, the same approach is followed: DLC 1.2 simulations are used to analyze the power production and fatigue loads during normal turbulence conditions, while DLC 1.3 simulations are used to analyze the ultimate loads reduction. These results are summarized in Table 38 and Table 39.

Component	Unit	REF	ETC	ratio [%]
DEQL blade flap	MNm	52.97	53.46	100.9
DEQL blade lead	MNm	71.98	71.92	99.93
DEQL blade XY	MNm	55.54	55.76	100.4
DEQL blade torsion	MNm	0.9832	0.9846	100.1
DEQL tower fore-aft	MNm	119.9	121	100.9
DEQL tower sideward	MNm	50.55	50.66	100.2
DEQL tower XY	MNm	119.7	120.7	100.8
DEQL shaft Y	MNm	30.4	30.3	99.57
DEQL shaft Z	MNm	30.5	30.3	99.49
DEQL shaft YZ	MNm	18.4	18.4	99.71
DEQL tower top tilt	MNm	23.9	23.8	99.68
DEQL tower top yaw	MNm	22.8	22.7	99.63
Energy capture 10-min	MWh	1.86	1.85	99.43

Table 38 Summary of energy yield and 600-cycles damage equivalent loads for INNWIND 20MW RWT based on DLC 1.2

Table 38 reports a power production loss of just above 0.5% in DLC 1.2, which is somewhat higher than the value using during the ETC design (0.4%). Such small differences are possible since the ETC optimization procedure is performed based on simulations without ETC and cannot exactly predict the effects of closing the ETC loop. The fatigue loads with ETC are kept similar to these in the reference case, although some minor increase (of less than 1%) is observed at the tower. Altogether more or less acceptable performance degradation in DLC 1.2, provided that significant reduction of ultimate loads is realized in DLC 1.3.

Component	Unit	REF	ETC	ratio [%]
EXTR blade flap	MNm	163.6	158.1	96.65
EXTR blade lead	MNm	87.39	85.23	97.53
EXTR blade XY	MNm	174.7	165.8	94.89
EXTR blade torsion	MNm	2.023	2.152	106.4
EXTR tower fore-aft	MNm	931.7	920.5	98.8
EXTR tower sideward	MNm	320.7	360.9	112.5
EXTR tower XY	MNm	948	921.4	97.19
EXTR shaft Y	MNm	131	108	**82.43**
EXTR shaft Z	MNm	109	110	100.9
EXTR shaft YZ	MNm	140	118	**84.2**
EXTR tower top tilt	MNm	145	121	**83.89**
EXTR tower top yaw	MNm	108	106	97.88
EXTR tip deflection	m	18.3	18.1	98.81

Table 39 Summary of ultimate loads for InnWind 20MW RWT based on DLC 1.3

The effect on the ultimate loads is reported in Table 39. Clearly, the loads reduction now is much less pronounced than was the case with the INNWIND 10MW RWT (compare to Table 36). Blade and tower loads are reduced by just a few percent. Although a more prominent load reduction of almost 16% is achieved for the shaft loads, it was the tower and blade loads for which the ETC algorithm has been optimized here. If the focus would have been on the shaft loads instead, then the ETC detection threshold would have been optimized for higher wind speeds where the shaft loads are highest (see bottom right-hand side plot in Figure 34. In that case the shaft loads are expected to be reduced even further than the 15% now for the same power loss tolerance, while the effect on blade and tower loads would practically disappear.

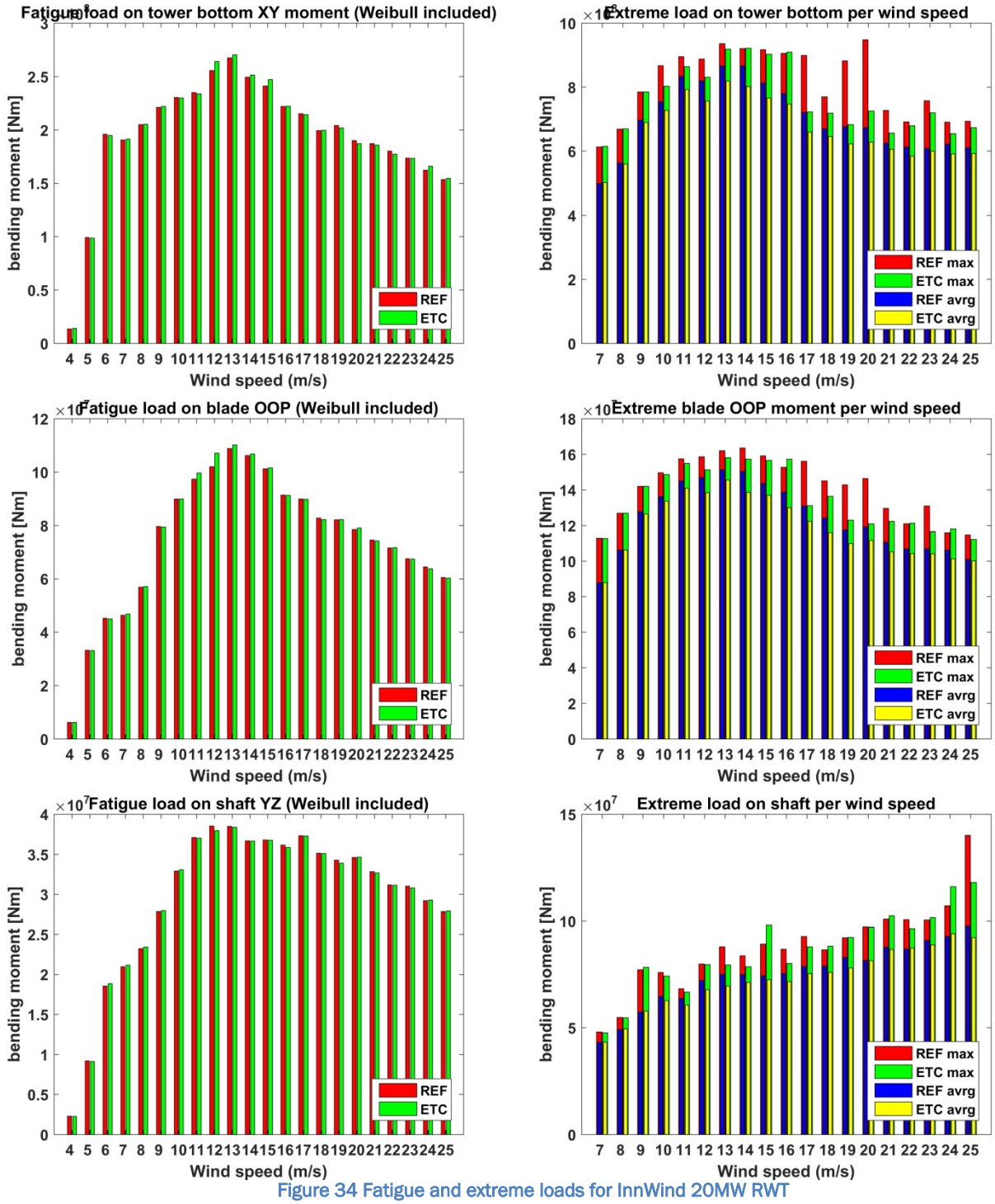

Figure 34 Fatigue and extreme loads for InnWind 20MW RWT

5.3 Discussion

Based on the performed evaluations using the INNWIND 10MW and 20MW RTW models it can be concluded altogether that by accepting small power loss (about 0.5% on annual basis) during normal production, the ultimate loads during extreme turbulence conditions can be reduced by more than 20% provided that the highest loads occur at high wind speeds well above rated.

Possible further improvements are expected if the rotor speed reduction offset is made wind speed dependent. This would allow reducing the rotor speed more for wind speeds at which the ultimate loads occur, thereby limiting power production losses even further. Another possible extension would be to allow for different levels of turbulence, i.e. by using a set of detection thresholds and corresponding derating strategies. This might be particularly of interest in wind farms where the local turbulence conditions strongly depend on the wind direction. Further, an alternative approach could be to base the detection logic on other measurements, rather than the estimated rotor effective wind speed. For instance, using measurements of the incoming air flow (e.g. with metmasts or LiDARs) are expected to be even more effective. Using vibrations and/or loads measurements could also prove to be an equally effective approach, removing the necessity for have a wind speed estimator.

7.0 Quantification of LCOE Reduction of Innovations at 10 MW and 20 MW Scale with Advanced Control (ALL)

Two methods of flap control have been studied, IFC + IPC (IFPC) using blade root load feedback and intelligent shutdowns and IFC with the flap controller using inflow measurements from a spinner mounted anemometer for a feedforward approach (IFPC-FF). Both types of IFC control have been applied to the 20 MW 3-bladed rotor on a jacket and to the 10 MW 2 bladed rotor on a semi-floater. While the IFC and IPC control features significantly reduce fatigue and extremes, the tower base fatigue is reduced to a small extent. Since the jacket is primarily designed to meet fatigue life targets and since the jacket cost is much higher than the blade costs, the effect on LCOE due to the use of IFPC on the 20 MW on jacket is minimal. The increased energy capture due to the larger rotor of the LIR directly contributes to lower LCOE, that is a 3% increase in AEP due to the LIR contributes to a 3% reduction LCOE. The IFPC and IPC control aid in limiting the design loads, so that the increase in AEP does not result in an increase in design loads over the reference design.

The 2-bladed rotor on the semi-floater displayed about 0.5% reduction in LCOE due to IFC and about 3.4% reduction in LCOE due to the 8% increased rotor using the optimized blades. Therefore a combination of the optimized blades and IFC can result in about 4% reduction in LCOE for the 2-bladed 10 MW turbine compared to its reference. Therefore in both the 3-bladed rotor mounted on the jacket and the 2-bladed rotor on semi-floater, it was seen that the reduction in LCOE is due to increased energy capture with constrained loads rather than CAPEX savings due to load mitigation.

With regards to the 10 MW floating turbine, the effects of IFC and IPC resulted in reduction in blade root bending moments, tower top and tower base bending moments. However the reductions in extreme and fatigue loads are not of a high magnitude so as to warrant significant CAPEX savings. There can be savings in OPEX costs due to reduced fatigue in the mooring lines.

8.0 Conclusions

Individual flap with pitch control, IFPC has been compared to Individual pitch control, IPC on the INNWIND 20 MW RWT on an advanced steel jacket. The IFPC and IPC controllers are tuned to give similar results in fatigue load calculations and then IFPC is designed to reduce extreme loads during shutdowns that are caused by asymmetric rotor loading. Design loads are driven by DLC 1.4. When DLC 1.4 is included in the DLC's analysed, hub yaw loading is reduced by 4%, tower base torsional loading is reduced by 4.4%, mudline member torsional loads are reduced 9.4% and corner member loads are reduced 11.6%.

The 2-bladed 10 MW rotor with an optimized blade with 8% increased radius shows an increase in AEP of 3.4% and reduced tower base loads (fore-aft 12% and side-side 6.3%), resulting in improved fatigue life of the Semi Floater structure. IPFC on the 10 MW floating turbine showed marginal reductions in support structure extreme and fatigue loads, but may also result in longer mooring line life.

It was also demonstrated that ultimate loads incurred during operation in extreme turbulence conditions can be reduced by detection of the turbulence level and reduction of the rated rotor speed. Best results were obtained when the highest loads occur at high wind speeds well above rated, because the algorithm alertness can be increased there significantly at the expense of only moderate power production loss.

Overall the benefit to LCOE reduction from advanced controls was to be able to increase AEP with longer blades without resulting in increased design loads.

Bibliography

[1] "WP4 deliverable for floating concept,".

[2] Bæk P., "Unsteady Flow Modeling and Experimental Verification of Active Flow Control Concepts for Wind Turbine Blades, DTU RISOE, 2011. PhD Thesis.,".

[3] T., Manolas, D.I., Machairas, T., Karakalas, A., Riziotis, V.A., Saravanos, D., Voutsinas, S.G., Tsiantas, "Assessment of fatigue load alleviation potential through blade trailing edge morphing," *Proceedings of the Science of Making Torque from Wind Conference, TORQUE 2016, Munich, Germany, 5-7 October*.

[4] J.W., Rasmussen, F., van Wingerden, "Wind tunnel and mid-sized wind turbine tests," Innwind.EU deliverable report 2.3.3, 2017".

[5] "Delivearble D2.14, New aero-structure rotor concepts and evaluation for 20 MW turbines, INNWIND.EU, 2017,".

[6] "Deliverable D4.13, Innovations on component level, INNWIND.EU, 2015,".

[7] "Deliverable D2.11, New aerodynamics rotor concepts specifically for very large offshore wind turbines, INNWIND.EU, 2013,".

[8] "Deliverable D1.43, Methods for feed-forward control and real time system simulator, INNWIND.EU 2017,".

[9] Deliverable D4.34, Innovative Design of a 10MW Steel-Type Jacket, INNWIND.EU, 2016.

[10] Bossanyi E. Individual blade pitch control for load reduction. Wind Energy 2003; 6:119–128.

[11] C. E. Plumley, "Increasing the Acceptance of Wind Turbines with Smart Rotor Control, University of Strathclyde, 2014.".

[12] M. H. Hansen and L. C. Henriksen, "Basic DTU Wind Energy controller, DTU Wind Energy E-0018, 2013.".

[13] "Deliverable D2.3.2,Validation of New Control Concepts by Advanced Fluid-Structure Interaction Tools, INNWIND.EU, 2015,".

[14] "Deliverable D1.25, 20 MW Reference Wind Turbine, INNWIND.EU, 2016,".

[15] IEC. IEC 61400-1. Wind turbines – Part 1: Design Requirements, 2005.

[16] IEA, "Wind turbines - Part 3: Design requirements for offshore wind turbines, no. IEC 61400-3. 2009.".

[17] C. Bottasso, A. Croce, C. Riboldi, and M. Salvetti, "Cyclic pitch control for the reduction of ultimate loads on wind turbines," in *The Science of Making Torque from Wind Conference*, 2014.

[18] E. Bossanyi, "Wind Turbine Control for Load Reduction," *Wind Energy*, pp. 229-244, 2003.

[19] E. Bossanyi, A. Wright, and P. Fleming, "Further progress with field testing of individual pitch control," in *Proceedings of the European Wind Energy Conference*, 2010.

[20] S. Kanev and T. van Engelen, "Exploring the Limits in Individual Pitch Control," in *Proceedings of the European Wind Energy Conference (EWEC)*, 2009.

[21] S. Kanev et al., "Sustainable control. A new approach to operate wind turbines. Final public report.," 2012.

[22] S. Kanev and T. van Engelen, "Wind Turbine Extreme Gust Control," *Wind Energy*, pp. 18-35, 2010.

[23] E. Bossanyi, G. Ramtharan, and B. Savini, "The Importance of Control in Wind Turbine Design and Loading," in *Proceedings of the 17th Mediterranean Conference on Control and Automation*, 2009.

[24] C. Bak et al., "Description of the DTU 10 MW Reference Wind Turbine," 2013.

[25] J. Darrow, K. Johnson, and A. Wright, "Design of a tower and drive train damping controller for the three-bladed controls advanced research turbine operating in design-driving load cases," *Wind Energy*, pp. 571–601, 2011.

[26] W. Engels, S. Subhani, H. Zafar, and F. Savenije, "Extending wind turbine operational conditions; a comparison of set point adaptation and LQG individual pitch control for highly turbulent wind," *Proceedings of The Sciense of Making Torque from Wind (TORQUE 2014)*, 2014.

[27] P. Chaviaropoulos and A. Milidis, "20 MW Reference Wind Turbine Aeroelastic data of the onshore version," 2016.

[28] K. Østergaard, P. Brath, and J Stoustrup, "Estimation of effective wind speed," in *Proceedings of the conference on the science of making torque from wind*, 2007.

[29] S. Kanev, J. Schuurmans, R. Rutteman, and E. Nguyen, "Towards new industrial software for advanced wind turbine control," in *Proceedings of the EWEA conference*, 2011.

Appendix A Load case definition for 20 MW Reference Turbine (GL-GH, now DNV GL (UK))

General Comments

Fatigue results have been combined assuming:

- Wind with annual mean speed of 10 m/s (Class IC) and Weibull distribution.
- Wind directional probability is equal about 12 sectors (360°), so results from four directions (0-90°) can be combined.
- Start-up fatigue loads are accounted for by doubling the fatigue loading from normal shutdown simulations.

Excluded cases have been judged to not meaningfully contribute to lifetime DEL's.

Excluded extreme load cases are assumed not to be driving.

Certain control system failure cases have been excluded as alarm logic renders those failure modes to be benign or equivalent to existing load cases.

Fatigue Load Cases

Design load case:	1.2
Operating condition:	Power production
Wind conditions:	Normal turbulence model, $V_{in} < V_{hub} < V_{out}$
Sea conditions:	Normal sea state, no currents, MSL
Type of analysis:	Fatigue
Partial safety factors	Partial safety factor for fatigue

Description of simulations:

	Wind conditions				Wave conditions		Other	
	Vhub (m/s)	Long. TI (%)	Lat. TI (%)	Vert. TI (%)	Hs (m)	Tp (s)	Yaw Error (°)	Hours per year
1.2aax1-2	4	25.80%	20.64%	12.90%	1.10	5.88	-8	175.3
1.2abx1-2							0	175.3
1.2acx1-2							8	175.3
1.2bax1-2	6	20.20%	16.16%	10.10%	1.18	5.76	-8	411.2
1.2bbx1-2							0	411.2
1.2bcx1-2							8	411.2
1.2cax1-2	8	17.40%	13.92%	8.70%	1.31	5.67	-8	440.5
1.2cbx1-2							0	440.5
1.2ccx1-2							8	440.5
1.2dax1-2	10	15.72%	12.58%	7.86%	1.48	5.74	-8	415.7

1.2dbx1-2							0	415.7
1.2dcx1-2							8	415.7
1.2eax1-2	12	14.60%	11.68%	7.30%	1.70	5.88	-8	353.7
1.2ebx1-2							0	353.7
1.2ecx1-2							8	353.7
1.2fax1-2	14	13.80%	11.04%	6.90%	1.91	6.07	-8	274.9
1.2fbx1-2							0	274.9
1.2fcx1-2							8	274.9
1.2gax1-2	16	13.20%	10.56%	6.60%	2.19	6.37	-8	196.6
1.2gbx1-2							0	196.6
1.2gcx1-2							8	196.6
1.2hax1-2	18	12.73%	10.18%	6.37%	2.47	6.71	-8	130.0
1.2hbx1-2							0	130.0
1.2hcx1-2							8	130.0
1.2iax1-2	20	12.36%	9.89%	6.18%	2.76	6.99	-8	79.8
1.2ibx1-2							0	79.8
1.2icx1-2							8	79.8
1.2jax1-2	22	12.05%	9.64%	6.03%	3.09	7.40	-8	45.5
1.2jbx1-2							0	45.5
1.2jcx1-2							8	45.5
1.2kax1-2	24	11.80%	9.44%	5.90%	3.42	7.80	-8	24.2
1.2kbx1-2							0	24.2
1.2kcx1-2							8	24.2
Comments:	Three dimensional three component Kaimal turbulent wind field (600 s sample). Normal sea state with irregular waves defined using JONSWAP spectrum (Peakedness = 1). Wind gradient exponent (exponential model), α = 0.14. Mean sea level of 50 m. Two seeds per speed and yaw error indexed 1-2. Simulations run with 4 wind directions in 30° sectors around the structure from 0 - 90° (indexed x=a-d). Supervisory control is disabled for these simulations.							

Design load case (DLC):	2.4
Operating condition:	Power production followed by a control system fault
Wind conditions:	Normal turbulence model at Vr and Vout
Sea conditions:	Normal sea state, no currents, MSL
Type of analysis:	Fatigue
Partial safety factors	Partial safety factor for fatigue

Description of simulations:

	Wind conditions				Wave conditions		Other	
	Vhub (m/s)	Long. TI (%)	Lat. TI (%)	Vert. TI (%)	Hs (m)	Tp (s)	Fault	Occurences/Hours per year per seed
2.4aax1-6	11.4	14.89%	11.91%	7.45%	1.63	5.84	a	1.7
2.4abx1-6	25	11.68%	9.34%	5.84%	3.60	7.95	a	1.7
2.4bax1-6	11.4	14.89%	11.91%	7.45%	1.63	5.84	b	0.8
2.4bbx1-6	25	11.68%	9.34%	5.84%	3.60	7.95	b	0.8
2.4caxy1-6	11.4	14.89%	11.91%	7.45%	1.63	5.84	c	22.2
2.4cbxy1-6	25	11.68%	9.34%	5.84%	3.60	7.95	c	1.8

Comments:

Three dimensional three component Kaimal turbulent wind field (60 s sample).
Normal sea state with irregular waves defined using JONSWAP spectrum (Peakedness = 1).
Wind gradient exponent (exponential model), α = 0.14
Mean sea level of 50 m.
Six seeds per speed indexed 1-6.
Simulations run with 4 wind directions in 30° sectors around the structure from 0 - 90° (indexed x=a-d)
Fault occurs 20 s into simulation.
Faults considered:
a) Grid loss
b) Transducer error, n4 trip
c) Oblique inflow, i.e. max wind direction from North that control system allows before shutdown. Assumption: 24h per year under these conditions. Indexed y = a/b for +/- yaw. Amplitudes of 46°, 37°. Simulations run with 4 wind directions in 30° sectors around the structure from 0 - 90° (indexed x=a-d). Supervisory is disabled.

Design load case (DLC): 4.1
Operating condition: Normal shutdown
Wind conditions: Normal wind profile
Sea conditions: Normal sea state, no currents, MSL
Type of analysis: Fatigue
Partial safety factors Partial safety factor for fatigue

Description of simulations:

	Wind conditions		Wave conditions		Other
	Vhub (m/s)	Wind Direction (deg)	Hs (m)	Tp (s)	Occurrences/Hours per year
4.1ax	4	0.00	1.10	5.88	2000
4.1bx	11.4	0.00	1.63	5.84	100
4.1cx	25	0.00	3.60	7.95	100

Comments:

Steady wind 70 s simulations

Normal sea state with irregular waves defined using JONSWAP spectrum.

Simulations run with 4 wind directions in 30deg sectors around the structure from 0 - 90deg (indexed x=a-d)

Wind gradient exponent (exponential model), $\alpha = 0.14$

Mean sea level of 50 m

Design load case (DLC):	6.4
Operating condition:	Parked (stand still or idling)
Wind conditions:	Normal turbulence model, V_{hub} < 0.7 V_{ref}
Sea conditions:	Normal sea state, no currents, MSL
Type of analysis:	Fatigue
Partial safety factors:	Partial safety factor for fatigue

Description of simulations:

	Wind conditions				Wave conditions		Other	
	Vhub (m/s)	Long. TI (%)	Lat. TI (%)	Vert. TI (%)	Hs (m)	Tp (s)	Yaw Error (°)	Hours per year
6.4aax1-2	2	42.60	34.08	21.30	1.07	6.03	-8	345.1
6.4abx1-2							0	345.1
6.4acx1-2							8	345.1
6.4bax1-2	30	11.24	8.99	5.62	4.46	8.86	-8	21.5
6.4bbx1-2							0	21.5
6.4bcx1-2							8	21.5

Comments:

Three dimensional three component Kaimal turbulent wind field (600 s sample).
Normal sea state with irregular waves defined using JONSWAP spectrum (Peakedness = 1).
Wind gradient exponent (exponential model), α = 0.14.
Mean sea level of 50 m.
Two seeds per speed and yaw error indexed 1-2.
Simulations run with 4 wind directions in 30° sectors around the structure from 0 - 90° (indexed x=a-d).
Idling pitch angle of 90°.
Supervisory control is disabled for these simulations.

Extreme Load Cases

Design load case (DLC):	1.3
Operating condition:	Power production
Wind conditions:	Extreme turbulence model, $V_{in} < V_{hub} < V_{out}$
Sea conditions:	Normal sea state, no currents, MSL
Type of analysis:	Ultimate
Partial safety factors	Normal

Description of simulations:

	Wind conditions				Wave conditions		Other
	Vhub (m/s)	Long. TI (%)	Lat. TI (%)	Vert. TI (%)	Hs (m)	Tp (s)	Yaw Error (°)
1.3aa1-6	9.4	26.56%	21.25%	13.28%	1.43	5.72	-8
1.3ab1-6							0
1.3ac1-6							8
1.3ba1-6	11.4	23.11%	18.49%	11.56%	1.63	5.84	-8
1.3bb1-6							0
1.3bc1-6							8
1.3ca1-6	13.4	20.70%	16.56%	10.35%	1.85	6.01	-8
1.3cb1-6							0
1.3cc1-6							8
1.3da1-6	20	16.15%	12.92%	8.08%	2.76	6.99	-8
1.3db1-6							0
1.3dc1-6							8
1.3ea1-6	25	14.30%	11.44%	7.15%	3.60	7.95	-8
1.3eb1-6							0
1.3ec1-6							8

Comments:

Three dimensional three component Kaimal turbulent wind field (600 s sample).
Normal sea state with irregular waves defined using JONSWAP spectrum (Peakedness = 1).
Wind gradient exponent (exponential model), α = 0.14.
Mean sea level of 50 m.
Six seeds per speed and yaw error indexed 1-6.
Simulations run with 1 wind directions 0 °
c = 2.
The characteristic loads for each load case group are calculated as the mean of the maxima from each of the six seeds.
Supervisory control is disabled for these simulations.

Design load case (DLC):	1.4
Operating condition:	Power production
Wind conditions:	Extreme coherent gust with change of direction (ECD)
Sea conditions:	Normal sea state, no currents, MSL
Type of analysis:	Ultimate
Partial safety factors	Normal

Description of simulations:

	Wind conditions				Wave conditions		Other
	Vhub (m/s)	ΔV (m/s)	V_{end} (m/s)	Direction change (°)	Hs (s)	Tp (s)	Yaw Error (°)
1.4aaa_x_z	9.4	15	24.4	25.53	1.43	5.72	-8
1.4aab_x_z							0
1.4aac_x_z							8
1.4aba_x_z	9.4	15	24.4	51.07	1.43	5.72	-8
1.4abb_x_z							0
1.4abc_x_z							8
1.4aca_x_z	9.4	15	24.4	76.60	1.43	5.72	-8
1.4acb_x_z							0
1.4acc_x_z							8
1.4baa_x_z	11.4	15	26.4	21.05	1.63	5.84	-8
1.4bab_x_z							0
1.4bac_x_z							8
1.4bba_x_z	11.4	15	26.4	42.11	1.63	5.84	-8
1.4bbb_x_z							0
1.4bbc_x_z							8
1.4bca_x_z	11.4	15	26.4	63.16	1.63	5.84	-8
1.4bcb_x_z							0
1.4bcc_x_z							8
1.4caa_x_z	13.4	15	28.4	17.91	1.85	6.01	-8
1.4cab_x_z							0
1.4cac_x_z							8
1.4cba_x_z	13.4	15	28.4	35.82	1.85	6.01	-8
1.4cbb_x_z							0
1.4cbc_x_z							8
1.4cca_x_z	13.4	15	28.4	53.73	1.85	6.01	-8
1.4ccb_x_z							0
1.4ccc_x_z							8

Comments:	Steady wind with speed and direction transient (rise time = 10s). Normal sea state with irregular waves defined using JONSWAP spectrum (Peakedness = 1). Wind gradient exponent (exponential model), α = 0.14. Half type transient occurs 10 s into simulation. 200 s simulations. Mean sea level of 50 m. Direction change applied positively (indexed x=1) and negatively (indexed x=2). Simulations run with 1 wind directions 0°. Starting azimuth angle varied from 0-90° in 30° intervals (indexed z =1-4).

Design load case (DLC):	2.1
Operating condition:	Power production plus occurrence of fault
Wind conditions:	Normal turbulence model, $V_{in} < V_{hub} < V_{out}$
Sea conditions:	Normal sea state, no currents, MSL
Type of analysis:	Ultimate
Partial safety factors	Normal

Description of simulations:

	Wind conditions		Wave conditions		Other
	Vhub (m/s)	Long. TI (%)	Hs (s)	Tp (s)	Fault
2.1aa01-12	9.4	16.14	1.43	5.72	a
2.1ab01-12					b
2.1ac01-12					c
2.1ba01-12	11.4	14.89	1.63	5.84	a
2.1bb01-12					b
2.1bc01-12					c
2.1bd01-12					d
2.1be01-12					e
2.1ca01-12	13.4	14.01	1.85	6.01	a
2.1cb01-12					b
2.1cc01-12					c
2.1cd01-12					d
2.1ce01-12					e
2.1da01-12	20	12.36	2.76	6.99	a
2.1db01-12					b
2.1dc01-12					c
2.1dd01-12					d
2.1de01-12					e
2.1ea01-12	25	11.68	3.60	7.95	a
2.1eb01-12					b
2.1ec01-12					c
2.1ed01-12					d
2.1ee01-12					e

Comments:	Three dimensional three component Kaimal turbulent wind field (3 min sample). Normal sea state with irregular waves defined using JONSWAP spectrum (Peakedness = 1). Wind gradient exponent (exponential model), α = 0.14 Fault occurs 10 s into simulation Twelve turbulent wind fields used for each simulation, each using a different random number seed (indexed 1-12). Mean sea level of 50 m Simulations run with 1 wind directions 0 ° Faults: a) Controller failure. Over speed n4 trip tested b) Pitch angle deviation. Individual pitch runaway of blade 1 towards feather (recoverable) at 100% of hardware limit pitch rate c) Pitch angle deviation. Individual pitch runaway of blade 1 towards fine (recoverable) at 100% of hardware limit pitch rate d) Flap angle deviation. Individual flap runaway of blade 1 towards feather (recoverable) at 100% of hardware limit pitch rate. e) Flap angle deviation. Individual flap runaway of blade 1 towards fine (recoverable) 100% of hardware limit pitch rate. The characteristic loads for each load case group are calculated as the mean of the upper half of the maxima from each of the twelve seeds.

Design load case (DLC):	2.2
Operating condition:	Power production plus occurrence of fault
Wind conditions:	Normal turbulence model, $V_{in} < V_{hub} < V_{out}$
Sea conditions:	Normal sea state, no currents, MSL
Type of analysis:	Ultimate
Partial safety factors	Abnormal

Description of simulations:

	Wind conditions		Wave conditions		Other
	Vhub (m/s)	Long. TI (%)	Hs (s)	Tp (s)	Fault
2.2aa1-12	9.4	16.14	1.43	5.72	a
2.2ab1-12					b
2.2ac1-12					c
2.2ba1-12	11.4	14.89	1.63	5.84	a
2.2bb1-12					b
2.2bc1-12					c
2.2bd1-12					d
2.2ca1-12	13.4	14.01	1.85	6.01	a
2.2cb1-12					b
2.2cc1-12					c
2.2cd1-12					d
2.2da1-12	20	12.36	2.76	6.99	a
2.2db1-12					b
2.2dc1-12					c
2.2dd1-12					d
2.2ea1-12	25	11.68	3.60	7.95	a

2.2eb1-12					b
2.2ec1-12					c
2.2ed1-12					d
Comments:	Three dimensional three component Kaimal turbulent wind field (3 min sample). Normal sea state with irregular waves defined using JONSWAP spectrum (Peakedness = 1). Wind gradient exponent (exponential model), α = 0.14 Fault occurs 10 s into simulation Twelve turbulent wind fields used for each simulation, each using a different random number seed (indexed 1-12). Mean sea level of 50 m Simulations run with 1 wind directions 0 ° Faults: a) Controller failure. Over speed nA trip tested b) Control failure: collective pitch runaway towards fine at 100% of software limit pitch rate c) Pitch seizure. Single blade fails to pitch (3 min sample). d) Flap seizure. Single flap fails to pitch (3 min sample). The characteristic loads for each load case group are calculated as the mean of the upper half of the maxima from each of the twelve seeds.				

Design load case (DLC):	2.3
Operating condition:	Power production plus loss of electrical grid connection
Wind conditions:	Extreme operating gust (EOG)
Sea conditions:	Normal sea state, no currents, MSL
Type of analysis:	Ultimate
Partial safety factors	Abnormal

Description of simulations:

	Wind conditions		Wave conditions	
	Vhub (m/s)	EOG gust (m/s)	Hs (s)	Tp (s)
2.3ab_x_y	9.4	4.69	1.43	5.72
2.3bb_x_y	11.4	5.25	1.63	5.84
2.3cb_x_y	13.4	5.80	1.85	6.01
2.3db_x_y	20	7.64	2.76	6.99
2.3eb_x_y	25	9.03	3.60	7.95
Comments:	Steady wind with transient gust (gust period = 10.5s). 1 minute simulations Normal sea state with irregular waves defined using JONSWAP spectrum (Peakedness = 1). Wind gradient exponent (exponential model), α = 0.14 Gust occurs 10 s into simulation Internal or external electrical fault modelled as an instantaneous loss of the generator torque Mean sea level of 50 m Simulations run with 1 wind directions 0 ° Fault phasing indexed x=a-d corresponds to tstart gust +0, +2.45, +4.0 and +5.25s respectively. Starting azimuth angle varied from 0-90° in 30° intervals (indexed y=a-d). Wind direction is 0°			

Design load case (DLC):	4.2
Operating condition:	Normal shut-down plus deterministic gust
Wind conditions:	Extreme operating gust (EOG)
Sea conditions:	Normal sea state, no currents, MSL
Type of analysis:	Ultimate
Partial safety factors	Normal

Description of simulations:

	Wind conditions		Wave conditions	
	Vhub (m/s)	EOG gust (m/s)	Hs (s)	Tp (s)
4.2ab_x_y	9.4	4.69	1.43	5.72
4.2bb_x_y	11.4	5.25	1.63	5.84
4.2cb_x_y	13.4	5.80	1.85	6.01
4.2db_x_y	20	7.64	2.76	6.99
4.2eb_x_y	25	9.03	3.60	7.95

Comments:

Steady wind with transient gust (gust period = 10.5s). 1 minute simulations
Normal sea state with irregular waves defined using JONSWAP spectrum (Peakedness = 1).
Wind gradient exponent (exponential model), α = 0.14.
Gust occurs 10 s into simulation.
Mean sea level of 50 m.
Simulations run with 1 wind directions 0°.
Normal stop phasing indexed x=1-4 corresponds to tstart gust +0, +2.45, +4.0 and +5.25s respectively.
Starting azimuth angle varied from 0-90° in 30° intervals (indexed y=1-4).
Wind direction is 0°.